Ministry of Higher Education & Scientific Research

University Of Anbar

College of Engineering

BUCKLING AND POST BUCKLING ANALYSIS OF A COMPOSITE PLATE UNDER COMPRESSIVE LOADS

A Thesis

Submitted to the College of Engineering of

University Of Anbar in Partial Fulfillment

of the Requirements for the Degree of *Master* of Science

in

Mechanical Engineering

By

Suha Hashim Mohammed Aldosary

(Bachelor of Science in Mechanical Engineering 2007)

Supervised by:

Asst. Prof. Dr. Hamad M. Hasan

Rabi Al-Awwal 1443

October 2021

ABSTRACT

In the present study, nonlinear static stability analysis of orthotropic simply–supported laminated plates under uniaxial and biaxial compression loads is analytically investigated. The used laminated composite plates are made of unidirectional reinforced fiber (graphite) and matrix (epoxy), which are utilized in many advanced engineering structures.

The equations of motion for the laminated plates are derived using the first-order shear deformation plate theory (FSDT) with Von-Karman-type nonlinearity formulations and the minimum total potential energy principle. Thereafter, by displaying a two-step perturbation technique, the achieved nonlinear differential equations are solved. Then, the critical buckling loads and post-buckling equilibrium paths of the symmetrically laminated composites solved by Matlab software code.

Results are shown in the form of plots presenting the variation in dimensionless buckling load parameters with dimensionless maximum deflection. The validation of the proposed research was gained by comparing some numerical results with the other published researcher, in which offered a very good agreement with the presented results.

Furthermore, the effect of several parameters such as different biaxial loads, and aspect ratio (a/h) on the critical buckling loads and post-buckling equilibrium paths of graphite/epoxy orthotropic laminated plates are studied and detailed perceptibly. From the results, the maximum critical buckling loads are 217.9, and 111.6 under unequal biaxial compression loads, and under uniaxial load at (a/h) = 25, respectively. Also, the maximum post buckling strength of structure at unequal biaxial compression loads, and under uniaxial load at (a/h) = 25, respectively.

LIST OF CONTENTS

CHAPTER TWO LITERATURE REVIEW

CHAPTER THREE BASIC FORMULATIONS

CHAPTER FOUR RESULTS AND DISCUSSION

CHAPTER FIVE CONCLUSIONS

List of Figures

List of Tables

Abbreviations:

CLPT	= Classical Laminated Plate Theory
FSDT	= First Order Shear Deformation Theory
TSDT	= Third Order Shear Deformation Theory
HSDT	= Higher-Order Shear Deformation Theory
CPT	= Classical Plate Theory
CC	= Clamped-Clamped
PP	= Pinned-Pinned
CP	= Clamped-Pinned
FEM	= Finite Element Method
CFCF	= Clamped-Free-Clamped-Free
LCP	= Laminated Composite Plate
SSSS	= Simply Supported for all edges
CCSS	= Clamped and Simply Supported for plate edges
CCCC	= Clamped on all edges
IHSDT	= Inverse Hyperbolic Shear Deformation Theory
VSCL	= Variable Stiffness Composite Laminated Plates
MFDM	= Modified Feasible Direction Method
FGM	= Functionally Graded Materials
PFRC	= Piezoelectric Fiber-Reinforced Composite

Notations

Symbol	Notation	Unit
A	= plate length	M
B	= plate width	M
H	= plate thickness	M
x, y, z	= plate coordinates	M
u, v	= displacement components along x, y	M
w_0	= the deflection of the plate	M
E_1	= Longitudinal young's modulus	N/ m^2
E_2	= transverse young's modulus	N/ m^2
G_{012}	= in-plane shear modulus	N/ m^2
N_x, N_y, N_{xy}	= forces resultants	Newton
M_x, M_y, M_{xy}	= moments resultants	N. m
Q_y, Q_x	= transverse force resultants	Newton
ν	= volume fraction	Unitless
m	= axial wave number	Unitless
N	= circumferential wave number	Unitless
λ_x	= dimensionless stress resultants in x-direction	Unit less
λ_y	= dimensionless stress resultants in x-direction	Unit less

Matrix Notations:

$[A_{ij}]$	= Extensional stiffnesses matrix	N/ m^2
$[B_{ij}]$	= Bending-extensional stiffnesses matrix	N/ m^2
$[D_{ij}]$	= Bending stiffnesses matrix	N.m

CHAPTER ONE

INTRODUCTION

CHAPTER ONE

INTRODUCTION

1.1 INTRODUCTION

Composite materials are a combination of two or more materials. Most of the composites are made of two materials, where the reinforcement material is called ”Fiber”, and the base material is termed “Matrix”. The composite materials have many advantages like high stiffness, high strength, light weight, long fatigue life, plus excellent corrosion resistance (UnuthuReddy, 2003) [1].

As a result, the utilization of composite structures increases gradually for instance in aerospace, biomedicine, sport equipments, cars, medical instruments, building industry, ships, chemical industry, and other modern types of equipments, as shown in Figure 1-1(Pastuszak and Muc, 2013) [2].

Figure 1-1: Some applications of laminated composite materials (Rana, Parveen and Fangueiro, 2017) [3].

- ✓ Composite materials are commonly modeled in three types (Ye, 2002) [4], (Suliman, 2018) [5].

:

- ✓ Particulate composite, reinforcement particles in a matrix such as concrete, particles, in contrast to fibers, do not have a preferred orientation and can be either metallic or non-metallic as shown in Figure 1-2 (a).
- ✓ Fibrous composite, fibers in a matrix, the combination of fibers and a matrix can have high stiffness and strength, fibers can be long (continuous fiber) or short (usually randomly orientated fibers) or in many forms (unidirectional, woven, and bidirectional) as shown in Figure 1-2 (b and c).
- ✓ Laminated composite is a collection of laminae or plies that are bonded together and stacked to obtain the desired stiffness and thickness, with different orientations θ ($-90^o \leq \theta \leq 90^o$) as shown in Figure 1-2 (b). In this kind of composite the fiber orientation, and the thickness in each lamina function are key role of the mechanical properties of the composite. The sequence of different orientations of the plies in the laminated composite is called the stacking sequence as shown in Figure 1-3. The majority of laminated composite structures consist of unidirectional or woven fiber in the polymer matrix

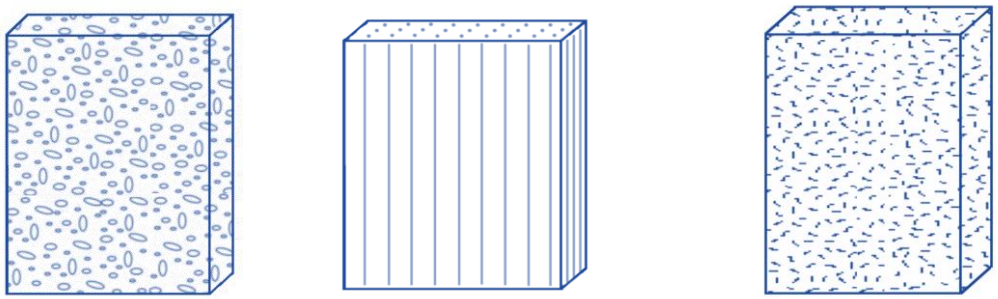

(a) (b) (c)

Figure 1-2: Categories of composite materials (a) Particulate composites (b) Continuous fiber-reinforced composites (c) Short random fiber reinforced composites. (Suliman, 2018) [5].

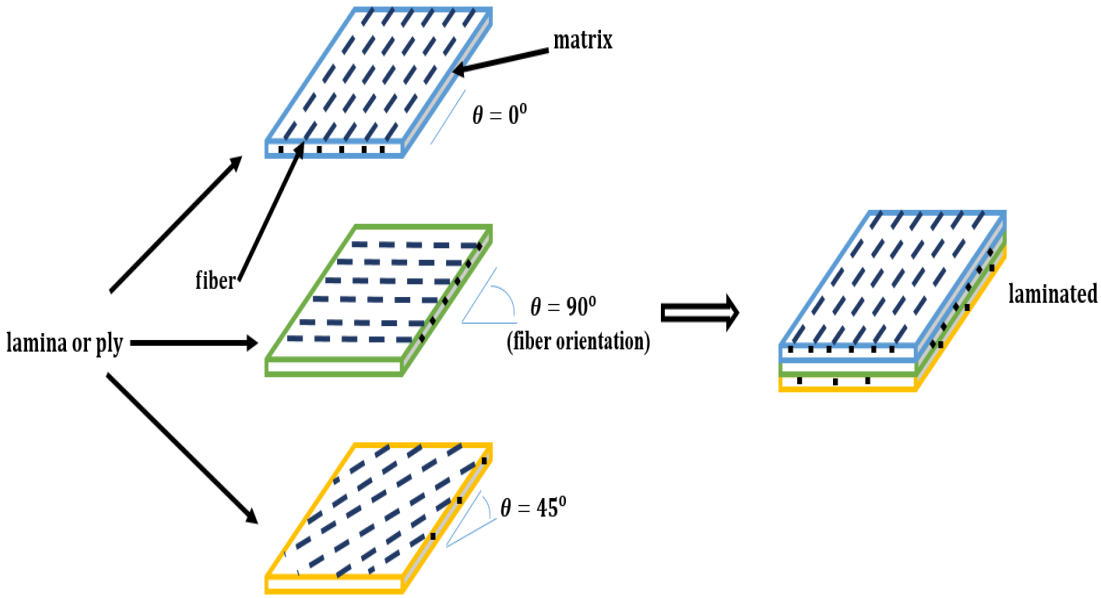

Figure 1-3: Composite laminate structure (Suliman, 2018) [5].

Laminates are categorized into cross-ply ($\theta = 0^o$ and 90^o) and angle ply (θ and $-\theta$) where ($0^o \leq \theta \leq 90^o$). These types may be symmetric, anti-symmetric, or un-symmetric (asymmetric). A laminate is called symmetric if the material, thickness, and angle of laminae are the same above and below the mid plane as shown in Figures (1-4) and (1-5). The materials of laminates (both fiber and matrix) can be isotropic, anisotropic, and orthotropic. The orthotropic materials are interesting and of great importance in the fields of modern industrial applications because of their features such as hardness, superelasticity, and lightness. Orthotropic materials are anisotropic materials with an structural inhomogeneous. These materials have two or three orthogonal axes so that their mechanical properties are different along each axis (Daniel et al., 2006) [6], (Moubayed et al., 2014) [7].

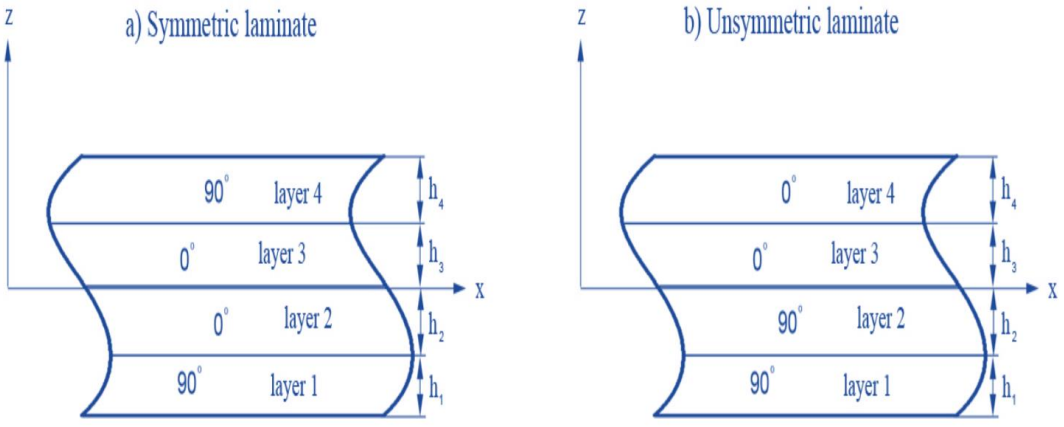

Figure 1-4: (a) symmetric cross-ply laminate and (b) un-symmetric cross-ply laminate (Turnock *et al.*, 2009) [8].

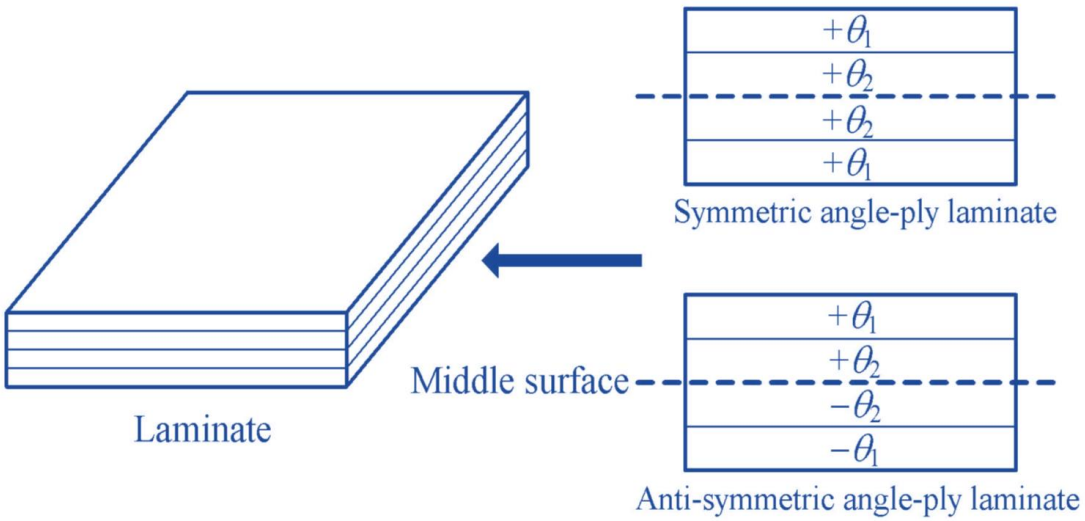

Figure1-5: Symmetric and anti-symmetric angle-ply laminates(Zhang, Zhang and Zhu, 2011) [9].

1.2 REINFORCEMENTS AND MATRICES

The fibers-reinforcement lamina consists of several fibers embedded in the matrix. Fibers are much stronger and stiffer than the matrix in the laminated form and consider the members of major load-carrying. The matrix protects the fibers, transfers loads between fibers, and keeps fiber in the proper position and orientation. A matrix can be in many forms polymer, metal, ceramic. Polymer matrices such as polyester, epoxy, polysulfone, etc., these resins are reinforced with carbon /graphite, glass, boron, or aramid fibers (Ye, 2002) [4].

Graphite materials are widely utilized in many fields such as energy conversion, petroleum refining, and chemical industry due to their excellent corrosion resistance, conductivity, thermal shock resistance, and thermal conductivity.

Epoxy matrix has high specific strength, bond behavior, and excellent corrosion resistance. The graphite/epoxy composite has a higher tensile strength and higher modulus. The graphite/epoxy composite is simple in mass production and molding, which can decrease the production cost of materials (Yao et al., 2020) [10].

1.3 CHARACTERIZATION OF THE UNIDIRECTIONALLY LAMINATED PLATE

The unidirectional fiber is treated as an orthotropic material in which material symmetrical planes are parallel and transverse to the direction of the fiber. The material coordinate axes (X and Y) are taken to be parallel and transverse to the direction of the fiber, respectively in the plane of the lamina. The engineering constants of the unidirectional fiber-reinforced lamina can be determined by using the micromechanics approach based on the following assumptions (UnuthuReddy, 2003) [1]:

- ✓ The bonding between fibers and matrix is perfect.
- ✓ Fibers are parallel, and they are uniformly distributed throughout materials.
- ✓ The applied loadings are either parallel or perpendicular to the direction of the fiber.
- ✓ Both fibers and matrices obey Hook's law and they are isotropic.
- ✓ A matrix is free of microcracks.

1.4 BUCKLING AND POST-BUCKLING PHENOMENA

Composite structures are subjected to compressive load, during their operating, this load may exceed a safety value and this may accrue buckling which may lead to failure. The transition of the composite material from the stable state of equilibrium to unstable state is referred to structural instability or buckling. Buckling is an onset of instability. Buckling failure takes place in plates, shells, columns, and other engineering structures. Buckling behavior is an excellent indicator of safe operating conditions and effective designs for these structures. If the compressive loads are small, the structure will deform but it remains flat. The equilibrium of the structure is stable and this behavior is expressed in terms of equilibrium paths. With increasing the load just enough to keep flat or slightly bent, this form is termed as the critical load. The critical load is called buckling load which is the smallest value of the load that can produce buckling. The stable state of the structure is confused and it seeks an alternative equilibrium configuration attended by a change in the load-deflection behavior. Without severe changes in deformation and the changing equilibrium configuration at the same load, this phenomenon is called bifurcation. The bifurcation point defines the point where buckling load is reached. The load-displacement curve can be divided into two steps, one pre-bifurcation point, and the other post-bifurcation point. When the compressive load is applied to the composite structure, the primary equilibrium path is obtained and it is stable until the bifurcation point has arrived. The primary equilibrium path of the structure becomes unstable after the bifurcation point.

The structure tries to find a secondary equilibrium path. In this stage, the secondary equilibrium path either can be post-buckling strength or post-buckling collapse as shown in Figure 1-6. A non-linear approach with large displacement is utilized to analyze the post-buckling behavior. (UnuthuReddy, 2003) [1], (Haugen, 2012) [11].

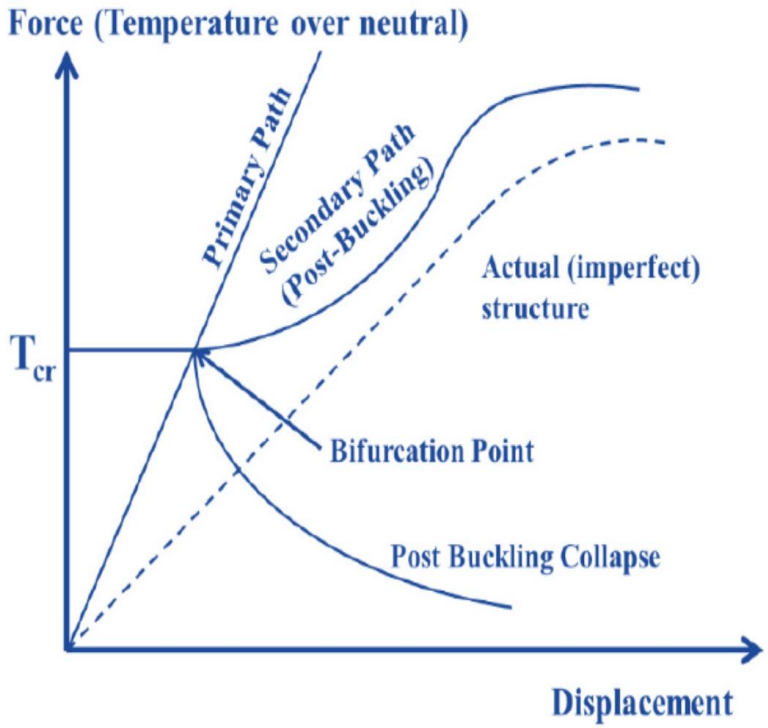

Figure 1-6: Buckling path (Ngamkhanong, Wey and Kaewunruen, 2020) [12].

1.5 DEVELOPMENTS IN THE THEORIES OF LAMINATED PLATES

Different plate theories have been developed by researchers as Classical Laminated Plate Theory (CLPT), First-order Shear Deformation Theory (FSDT), and higher-order Shear Deformation Theory (HSDT). A sound theoretical foundation is established by Von Karman for an isotropic rectangular thin plate that may be subject to finite deflection. This theory was later extended to the cases of nonlinear analysis of composite laminated thin plates. Many works deals with post-buckling, large deflection, and nonlinear analysis of composite laminated thin structures. In the classical plate theory (CPT) based on the Kirchhoff assumptions, the effect of transverse shear deformation is neglected. Recently, developments in the analysis of laminated composite plates offer that thickness of the plate has more pronounced effects on the influence of laminates composite than on the isotropic plates. When the rotary inertia and transverse shear effects are neglecting, that leads to incorrect results. To treat the influence of transverse shear deformation in plates is proposed a first-order shear deformation theory. This theory is then expanded to the cases of anisotropic plates. After the plate is deformed, the FSDT assumes that the mid-plane normal of the structure remains straight. This theory can represent constant transverse shear strains only through the thickness of the plate, violates the situations of vanishing of transverse shear stress at the bottom and top surfaces of the plates.

To compensate this requires the shear correction factor. Two types of higher-order shear deformation theory (HSDT) are proposed, to calculate the effect of the transverse normal strain. This theory satisfies the situations of vanishing of transverse share stress at the bottom and top surface of the plate. In HSDT, it is not required a shear correction factor (Vaikunthbhai, 2014) [13].

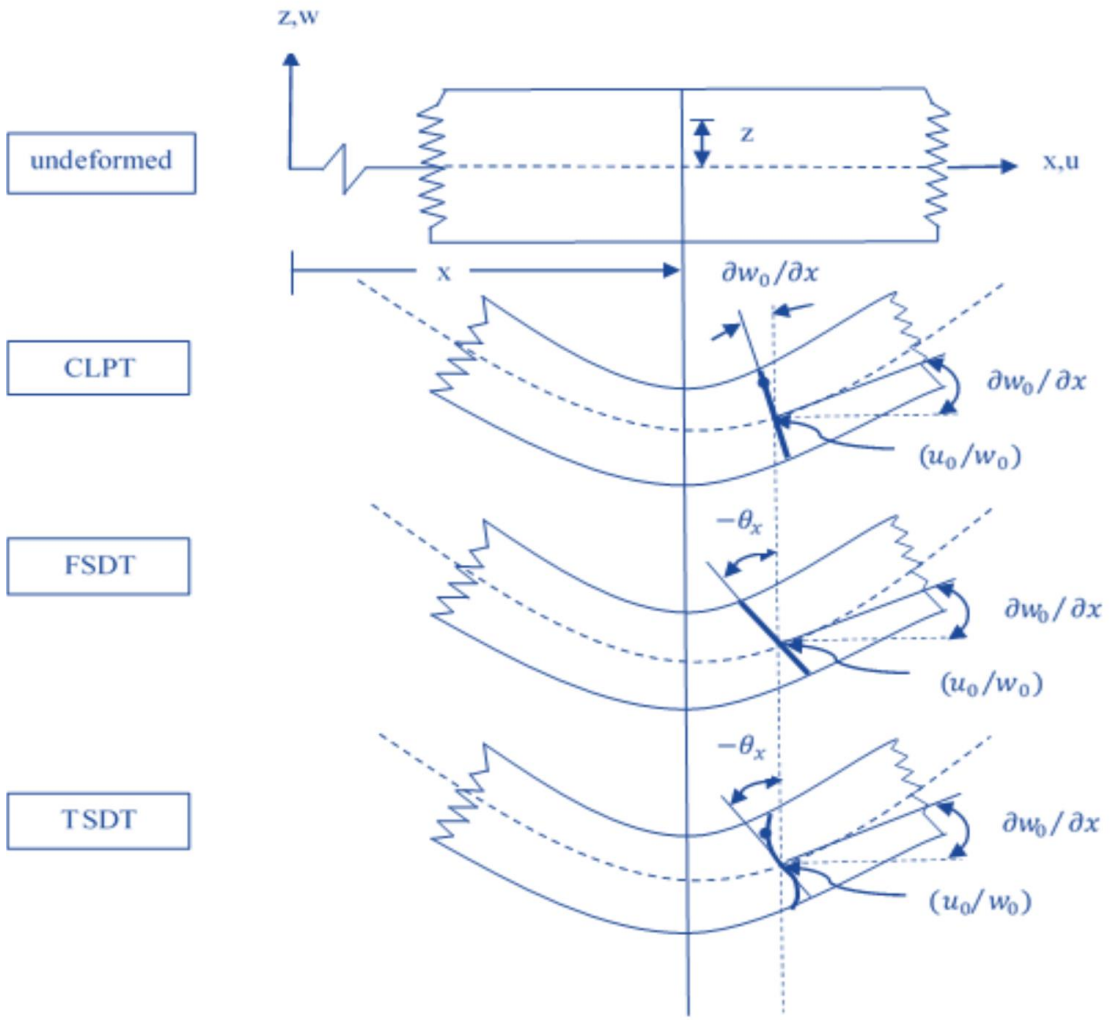

Figure 1-7: Deformation of a transverse normal according to the classical, first-order, and third-order plate theories (Vaikunthbhai, 2014) [13].

1.6 FIRST-ORDER SHEAR DEFORMATION

The first-order shear deformation theory has been used by many researchers due to its many advantages. It was established by Reissner and Mindlin. The assumptions of the first-order shear deformation plate theory can be divided into three parts. In the first part, after deformation, the transverse normal do not stay perpendicular to the mid surface but are inclined with an arbitrary angle in this way, transverse shear strains in direction (x_z) and (y_z) are included in the theory. This accounts for including transverse shear strain in the FSDT. In the second part, during deformation, the transverse normal is inextensible. In the last part, before and after deformation, displacement in direction (z) is constant in the thickness coordinate as shown in Figure 1-7. The FSDT requires shear correction factors to correct the discrepancy between the real stress state and the constant stress state considered by first-order shear deformation. The shear correction factor is used to modify the stiffness of laminated plate transverse shear. The shear correction factor depends on the geometric parameters, boundary conditions, lamination, and loading condition. For the homogeneous orthotropic plates, the shear correction factor K_s is considered as 5/6, (UnuthuReddy, 2003) [1], (Vrabie, Chiriac and Băetu, 2017) [14].

1.7 TWO-STEP PERTURBATION TECHNIQUE

This method is one of the most appropriate technique which can be used to solve different boundary-value problems in the elastic structures. It provides an advantageous of approximate analytical tool to solve a big class of nonlinear equations.

In the perturbation technique, the solution of the original equation is looked at as the sum of the solution of perturbation equations of each order and the sequence of terms as the increasing power of the small perturbation parameter with their coefficients. A two-step perturbation technique was firstly proposed by Zhang and Shen for post-buckling analyzes of isotropic plates. Later, this method was extended to analyse rectangular isotropic plates under uniaxial compressive load combined with lateral pressure. Then, the two-step perturbation method was used to analyze the post-buckling for orthotropic plates resting on a two-parameter elastic foundation. This method gives parametric analytical expressions of the changes in the post-buckling field and has been generalized to other plate post-buckling conditions. Shen derived the set of Von Karman- type equations which contain thermal effect, adopted on Reddy's higher-order shear deformation plate theory. This approach is successfully utilized for solving several post-buckling problems of composite laminated plates under the combined action of thermal, mechanical, and electric loads, with help of Von Karman-type equations. The advantage of this perturbation approach is that it provides solutions to accept both boundary conditions and governing equations carefully in the asymptotic sense. This method provides the behavior of all parameters and can be assessed easily on the solution. Galerkin and Ritz methods depend on the chosen admissible function that does not satisfy all the motion equations, natural boundary conditions, and geometrical parameters.

The two-step perturbation method is interesting because it can be utilized for structural nonlinear analysis in different fields such as nonlinear post-buckling, bending, and large amplitude vibration of the plate, shell, and beam structures. The successful application of the two-step method depends on the selection of the small perturbation parameter. The nondimensional deflection or the nondimensional load or both of these parameters are chosen as the perturbation parameter in this method (Shen, 2013) [15].

1.8 SCOPE OF THE WORK

The current study offers an analytical solution to investigate the buckling and post-buckling of the laminated composite plates (LCP) by using numerical analyses. The structure is under mechanical loading (uniaxial load and biaxial load). The theoretical formulations are derived by employing the first-order shear deformation theory plate. Then, the governing equations of motion are obtained based on the Two-Step perturbation technique method to give critical buckling loads and post-buckling equilibrium paths of perfect plate simply supported on all edges. The results are obtained numerically by using Matlab software. The laminated composite plate is consists of graphite fiber and thermoset epoxy.

1.9 AIM And OBJECTIVES

The present study aims to examine the buckling and post-buckling behaviors of an orthotropic laminated composite perfect plate under uniaxial and biaxial compressive loads. The designed structures are based on the first-order shear deformation theory to include transverse shear deformation effects with Von-Karman-type nonlinearity formulations, which are applied to develop the fundamental differential equations of the motion. The parametric investigation of the structure has been achieved by using the Two-Step perturbation technique analysis by using Matlab software.

The objectives that adopted to accomplish this study are:

- Employ the Two-Step Perturbation Technique, which was fully established to examine the stability of the structure.
- To study the effect of uniaxial loads on the critical buckling loads and Post-buckling equilibrium paths.
- To study the effect of different biaxial loads on the critical buckling loads and Post-buckling equilibrium paths.
- To explore the behavior of geometrical parameter length to thickness ratio (a/h) on the critical buckling loads and Post buckling equilibrium paths under uniaxial and equal biaxial loads.

1.10 THESIS OUTLINE

In the first chapter, composite materials, buckling, and post-buckling phenomena, developments in the theories of laminated plates, and two-step perturbation techniques are introduced.

In the second chapter, the studies which are related to buckling and post-buckling behaviors of composite laminates and various structures are reviewed.

In the third chapter, analytical solutions of buckling and post-buckling of composite laminated plate's model are investigated. Furthermore, first-order shear deformation theory includes transverse shear deformation effects with Von-Karman-type nonlinearity formulations are offered to derive the equation of motion. Then the two-step perturbation method is presented to obtain the critical buckling loads and post-buckling equilibrium paths in this chapter.

In the fourth chapter, the laminated graphite/epoxy plate's model was displayed and compared with previously published literature to verify the accuracy of the currently employed method with the obtained results. Then the results regarding the static buckling and post-buckling behavior is determined and analyzed under many parameters.

In the fifth chapter, this chapter includes the conclusions of the results, and the suggestions for future work.

CHAPTER TWO

LITERATURE REVIEW

CHAPTER TWO

LITERATURE REVIEW

2.1 INTRODUCTION

Designers take into consideration the buckling test during modeling structures. The effect of buckling and post-buckling influences on the laminated composite plates are examined by many researchers, who adopted analytical and numerical methods.

Laminated composite plates are designed based on different theories to investigate the stability of structures under mechanical loads. The major theories used to analysis the stability of laminated composite plates, include classical laminated plate theory, first-order shear deformation theory, and higher-order shear deformation theory.

In this chapter, a literature review will be divided into three sections to obtain the stability behavior: the first part presents different theories and methods of the laminated composite plate. The second part review includes researchers who offered the (FSDT). The last part explains the Two-Step perturbation technique method.

2.2 LAMINATED COMPOSITE PLATES

(Baba and Baltaci, 2007) [16] numerically and experimentally investigated the influence of buckling of Glass/Epoxy laminated composite plates under axial compressive loading. The study aimed to determine the effect of aspect ratio, boundary conditions, anti-symmetric configuration, and cutout on the buckling behavior of the structure. The present study examined two different laminates configurations ($[90^o, 45^o, -45^o, 0^o]_s$ and $[90^o,45^o,-45^o,0^o]_{as}$), ratio (L/t = 37.5 and 75) with three boundary conditions (Clamped-Clamped (CC), Pinned-Pinned (PP), and Clamped-Pinned (CP)). Firstly, the buckling loads of rectangular laminated eight-ply were experimentally examined. By ANSYS computer code of Finite Element (FE), the buckling loads of structure were calculated. It was shown with clamped boundary condition, the buckling loads are higher than the other.

(Kumar et al., 2009) [17] examined the buckling behavior of rectangular laminated composite plates, by using finite element method. The structure under in-plane loads with Clamped-Free-Clamped-Free (CFCF) boundary conditions. The objective of the study was to understand the effect of the aspect ratio, fiber angle, length-to-thickness ratio, the cut-out shape on the buckling load for the Glass/Epoxy laminated composite plate. It was found that the composite plate with $[45]_8$ layup had the lowest buckling load, while the plate with $[0]_8$ layup had the highest buckling loads.

(Tu et al., 2020) [18] conducted the analytical approach to examine the nonlinear buckling and post-buckling behavior of the imperfect thin porous plate. The plate was subjected to in-plane compressive loading. The classical plate theory with taking into consideration the initial geometrical imperfection and Von-Karman nonlinearity used to derive the equations of motion. Galerkin's method was adopted to obtain the closed-form expression of deflection-buckling load curves of a rectangular porous plate. There were two types of distribution porosity. The elastic moduli with porous material are assumed to change through the thickness of the rectangular plate according to the distribution kinds. The effect of aspect ratio, imperfection, boundary condition, porosity coefficient, changing porosity distribution on the post-buckling response of the structure was studied. The influenced post-buckling of porous plates was significantly behaved by these parameters. From the numerical results, the post-buckling curve of asymmetric porosity distribution was lower than those for nonlinear symmetric porosity.

(Hu, Badir and Abatan, 2003)[19] studied the buckling response of a rectangular symmetric laminated composite plate. The plate was subjected to parabolic variation of axial loading. It was composed of AS4 graphite fibers and 3501-6 epoxy matrix, and it was assumed anisotropy about its mid-plane. Classical laminated plate theory with Rayleigh-Ritz was based to obtain the analytical solution of mode shape and buckling load. There were two conditions of loading on an axial load with parabolically varies of a plate in the longitudinal direction and transverse direction. The fiber orientation and aspect ratio of the structure have been examined.

As seen from the results, with increasing the aspect ratio, the buckling load of the plate subject uniaxial compression constant was converged to constant, while the buckling load under the varying axial load is decreased.

(Wankhade and Niyogi, 2020) [20] discovered the buckling behavior of isotropic laminated composite plates for three-layered (0^o, 90^o, 0^o). The simplified form of governing motion equations was used to examine buckling analysis of structure. The Laminated Composite Plate (LCP) was under compressive load. The effect of various parameters on the buckling loads was studied like aspect ratio, E_1/E_2 ratio, boundary conditions, stacking sequences with different modes of buckling. The results explained that with the aspect ratio of the structure obtains doubled, the buckling forces lower down about 36% for the thin plates to moderately thick plates. The higher modes present the greater value of buckling loads.

(Fernandes and Mirje, 2018) [21] displayed the finite element numerical method to study the buckling behavior for the cross-ply symmetric laminated composite plate. The structure was subjected to mechanical compressive loading. The effects of a different parameter on critical buckling loads were examined such as aspect ratio, aspect ratio, number of layers, the orthotropic ratio (E_1/E_2), boundary conditions (SSSS), (CCSS), (CSCS), and (CCCC), fiber angle orientation, and stacking sequence. The results showed that for different aspect ratios and all boundary collections of boundary conditions, the orthotropic ratio increased lead to the critical buckling loads increase.

(Kulkarni and Dhurvey, 2014) [22] investigated the post-buckling behavior of symmetric angle-ply and cross-ply square laminated composite plates. They were based on the finite element ABAQUS to analyze the structure under uniaxial compressive load. Three materials were examined in the analysis Boron/Epoxy, Carbon/Epoxy, Graphite/Epoxy. The plate was under uniaxial loading in the longitudinal direction. Effects of various parameters were studied in the number of layers, fiber orientation angle, and the (E_1/E_2) ratio. The results indicated the modeling of the laminated composite plates. It was noticed, in the same central displacement, the buckling loads of a cross-ply were lower than that of an angle-ply.

(Sreehari and Maiti, 2015)[23] employed the Inverse Hyperbolic Shear Deformation Theory (IHSDT) to analyze the buckling and post-buckling behavior of laminated composite plates. This theory supplied the non-linear transfer shear stress distribution. Also, at the top and bottom surface of the structure, the (IHSDT) contented zero transverse shear stress conditions. They were based on the finite element method for handling instability structure under mechanic and hygrothermal loads. The geometric nonlinearity was taken into account in the Von-Karman sense. In the MATLAB environment, the programming and mathematical formulation have been done. The aspect ratio, and modulus ratioE_1/E_2, were examined to understand the buckling behavior under the various parameters. The main result was offered, the buckling load in biaxial cases was less than similar uniaxial cases and any modulus ratio was analyzed.

(Majeed and Tayeh, 2015) [24] studied free vibration and buckling analysis of rectangular laminated composite plate under uniform and non-uniform compressive loading. Classical laminated composite plate theory (CLPT) with Hamilton's principle was based on the derivation equation of motion. Ritz method was adopted to solve these equations as an Eigen-value problem to obtain buckling load. The buckling load of the laminated plate with various combinations of boundary conditions was examined and obtain. Analytical results were presented to bring out the effect of lamination angle, loading type, boundary condition, a spect ratio on the critical buckling load. The important result was noticed, natural frequency and critical buckling load were high at the clamped edge plates.

(Lengvarský, Bocko and Hagara, 2016) [25] adopted the finite element method (FEM) to examine the buckling analysis of rectangular laminated composite plates as four various orientations of layers. The laminated plate was loaded with shear load, compression load, and collection of both loads. Calculated critical buckling loads were compared for all orientation layers. The results offer the inappropriate orientations of layers were obtained for different loads. The boundary conditions with x and y directions on the parallel edges were applied. The computed critical buckling load showed for all configurations. The influences of the number of layers, angle of the fiber, and thickness of layers on the buckling behavior were studied. From the results, it was noticed with increasing the thickness of composite structure as well as numbers of layers, the critical buckling load increase.

(Torabizadeh, 2015) [26] used classical laminated plate theory (CLPT) and first-order shear deformation theory (FSDT) to solve the laminated composite plates subjected to mechanical loads. The Navier-type method was applied to analyze rectangular cross-ply and angle-ply simply supported laminated plate. Also, finite element ANSYS and verification methods were developed. Effects of the laminated scheme, number of layers, modulus ratio, lamination angle, plate aspect ratio, and axial load direction on the critical buckling loads of structure were also investigated. Some of the important conclusions were shown: for square angle-ply anti-symmetric laminated the bending-extension coupling severely decreases the buckling load under uniaxial and biaxial load.

(Osman and Suleiman, 2017) [27] investigated the Buckling analysis of symmetric cross-ply rectangular laminates plate under uniaxial and biaxial compression. Based on the classical laminate theory, they used finite element analysis to obtain the numerical solution of the equations of motion. The effect of elastic modulus ratio, aspect ratio (a/b), and boundary condition on buckling load was explained. It is found that as the laminated plate becomes more restrained its resistance when the buckling increases. The critical buckling load decreases with the modulus ratio increases and for higher values of the elastic modular ratio, the critical buckling load becomes almost constant.

2.3 FIRST-ORDER SHEAR DEFORMATION THEORY

(Ferreira et al., 2011) [28] utilized a first-order shear deformation theory plate to analyze a buckling of an isotropic and laminated composite plate. The structure was under partial in-plane edge loads. The wavelet collocation method was adopted to solve the buckling load. The results were compared with finite element schemes that find in a very good agreement. For a square isotropic plate under a uniaxial load of simply supported boundary conditions, the effect of shear deformation was significant and evident on the buckling parameter. The buckling of the cross-ply laminated plate under uniaxial was examined, results present the effect of the number of layers and degree of orthotropic of the layers individual on the critical buckling load. It is shown the current method produces highly exact critical load and modes.

(Shukla et al., 2005) [29] estimated the critical and buckling loads of rectangular cross-ply and angle-ply laminated composite plates. The structure was subject in-plane to uniaxial and biaxial loading. By using a first-order shear deformation theory plate with Von-Karman-type nonlinearity formulations the equations of motion were obtained. The linearization technique and spatial discretization schemes were described. The influence of aspect ratio, moduli ratio, and the number of layers, the orientation of fibers, boundary condition, symmetric-cross ply, and anti-symmetric angle-ply on the buckling behavior was studied and obtained results. With biaxial loading, a maximum buckling load occurs at a fiber angle of 45^{o}.

(El Bouhmidi and Rougui, 2018) [30] investigated the buckling behavior of E-Glass/Epoxy perforated symmetric and anti-symmetric composite laminated plates. The structure with the circular hole was subjected to uniaxial static loading. The first-order shear deformation theory plate and variational energy method were used in mathematical formulation to obtain the critical buckling load. The solutions were done with the finite element method. The buckling load depends on several factors such as different boundary conditions, aspect ratio, lay-up sequences, angle of ply orientation, and the diameter of the circular hole. The result offers in graphical form with different boundary conditions. Among these parameters boundary conditions of the plate obtained the strongest mark on the buckling load. The big hole under the loading causes the weakest plate.

(Shadmehri, Hoa and Hojjati, 2012) [31] employed the first-order shear deformation theory to derive the equations of motion. Ritz method is adopted to solve these equations, to obtain the linear buckling behavior of conical composite shells. The shell was subjected to axial compressive loading. Both axisymmetric and non-axisymmetric formulations are derived and solved for each laminated composite conical shell, the lowest buckling load was selected as a critical buckling load. The parameter is studied to find the effect on the critical buckling load like fiber orientation and cone angle. The derivation can be drawn from the different parameters examined presented in the numerical results. With the increased fiber orientation, the critical buckling load decrease at short conical shells and angle-ply thin shells.

(DOĞAN, 2020) [32] studied the buckling behavior of thin and thick laminated composite plates by applied first-order shear deformation theory with Hamilton's principle to drive the equations of motion. The loading condition of a simply supported symmetric rectangular plate was uniaxial and biaxial compressive loads. The solution was groped by applying the Navier solution technique. In this study, the effect of anisotropy and edge ratios on the buckling analysis of structure, aspect ratio, (E_1/E_2) ratio, and the number of layers were examined. The results of numerical studies for the buckling behavior of (LCP) are benchmarked and demonstrated with former papers in the literature and software ANSYS finite element method. It was found that, at (E_1/E_2) ratio change from 30 to 40, the non-dimensional buckling load increase.

2.4 TWO-STEP PERTURBATION TECHNIQUE

(The song et al., 2017) [33] studied the buckling and post-buckling attitude of functionally graded multilayer plates. The GPLRC was subjected to biaxial compressive loads. The two-step perturbation technique was used to examine the post-buckling solution both perfect and imperfect structure simply supported on edges. The equations of motion for plates were derived by utilizing a first-order shear deformation theory with taking into consideration both initial geometrical imperfection and geometrical nonlinearity in von Kármán sense. The effects of the total number of layers, as well as GPL weight fraction, geometry, and distribution pattern, on the buckling influence of structure, were determined in detail. The results have revealed that can significantly improve the attitude of buckling and post-buckling of the plates by dispersing a small amount of GPLs into the matrix.

(Shen, 2009) [34] employed the higher-order shear deformation theory plate to derive the motion equation. To determine a buckling load and post-buckling path a Two-Step perturbation technique is adopted. Shear deformable functionality graded (FGM) symmetric plate, simply supported as the piezoelectric fiber-reinforced composite (PFRC) actuator is examined. The nonlinear compressive and thermal post-buckling behaviors of the structure have been presented. The plate was under to uniform temperature rise or uniaxial compression combined with a load of electricity. The initial geometric imperfection of the structure was considered. The material properties of both PFRC and FGM layers were supposed to be temperature-dependent. The numerical illustrations concern the thermal and compressive post-buckling behavior of imperfect and perfect, symmetric FGM plates with embedded or fully covered PFRC actuators subjected to various sets of electric and thermal conditions. The negative voltage was used to decrease the deflection of post-buckling and increase the buckling load.

(Shen et al., 2017) [35] offered the Two-Step perturbation technique to examine the buckling load and post-buckling equilibrium paths of the functionally graded graphene-reinforced composite (FG-GRC_S) laminated plate. The structure resting on an elastic foundation was subjected to uniaxial compressive loading in a thermal environment. The post-buckling attitude of functionally graded grapheme-reinforced composite (FG- GRC_S) plate was designed by a Higher-Order Shear Deformation Plate Theory. The thermal effects and plate-foundation interaction were taken into consideration. The buckling behavior of imperfect and perfect, symmetric FG-GRC plates subjected to different conditions of the thermal environment was examined and obtain. The post-buckling strength of the GRC laminated structures was

significantly influenced by the transverse shear deformation, temperature rise, foundation stiffness, aspect ratio, and boundary conditions. A buckling load and post-buckling strength of the GRC laminated plate can be enhanced with the piece-wise FG distribution of graphene.

(Li, Liu and Yang, 2018) [36] displayed the Two-Step perturbation technique to examine the interaction buckling and post-buckling analysis for a thick moderately anisotropic laminated cylindrical shell. The structure under axial compression and external pressure, that extends the boundary layer theory of buckling shell. Equations of equilibrium derived by higher-order shear deformation shell theory with kinematic nonlinearity of Von-Karman Donnell. The initial imperfection and pre-buckling nonlinear deformation of the shell were considered. The internal physical mechanism of the structure's geometric different parameters on the buckling behavior and post-buckling strength was obtained. The numerical illustrations concern the post-buckling behavior of imperfect and perfect, anisotropic laminated cylinder shells, moderately thick with various load-proportional parameters. The shape of the buckling interaction curve base on the stacking sequence of the laminated shell significantly, parameters geometric shell, the number of layers. The results showed a powerful and new technique to solve a buckling problem of the structure shell by the effects of different complex loads.

(Shen and Xiang, 2018) [37] adopted a Two-Step perturbation technique to solve the equations of motion to obtain the buckling load and post-buckling strength for perfect and imperfect GRC laminated cylindrical shells. The structure was subjected to axial compressive loading in a thermal environment. The equation of motion derived by Reddy’s third-order shear deformation shell theory with Von-Karman kinematic nonlinear and effect

of temperature variation. The piece-wise of graphene-reinforced composite layers were formed in a functionally graded model along the thickness direction of the shells. The buckling load and post-buckling equilibrium path can be improved with the piece-wise FG distribution of graphene reinforcement. It was noticed: with axially-loaded graphene-reinforced composite laminated cylindrical shells have unstable equilibrium paths of post-buckling.

(Fan and Wang, 2016) [38] investigated the nonlinear vibration and thermal post-buckling of the post-buckled matrix cracked hybrid laminated plate with a Pasternak elastic foundation. The Tow-Step perturbation technique was based to get the governing equation. The interaction between the structure and elastic foundation was taken into consideration. The higher-order shear deformation plate theory and kinematic nonlinearity of Von-Karman were used to obtain the equations of motion. The structure was a composite of carbon nanotube-reinforced composite (CNTRC) layers and conventional fiber-reinforced composite (FRC) layers. The matrix cracks have an important effect on the linear frequencies and thermal post-buckling of the hybrid laminated composite plate. The effect of matrix crack was weak or maybe neglected for nonlinear vibration problems. The different parameter that examines was conducted to study the influence of FG distribution of CNT, matrix crack, foundation stiffness, and volume fraction of CNT on the thermal post-buckling of the cross-ply hybrid laminated plate. It was revealed, the width to thickness ratio made the effect more pronounced of matrix cracking on linear vibration of the plate with thermally post buckled.

(Shen and Li, 2004) [39] used the Two-Step perturbation technique to examine the post-buckling behavior of the shear deformable laminated plate. The structure was supported by a tensionless elastic foundation under compressive edge loading or the uniform temperature rise. The formulations were obtained by using higher-order shear deformation plate theory and the Von-Karman of kinematic nonlinear. The initial imperfection of the structure was taken into consideration. The thermal effects were also taken into account and the material properties are independent of temperature. The advantage of an analytical-numerical method was that the solving is in explicit form. In simple to program in computing non-linear load end shortening and load-deflection curves without prior assumption for the contact region of the shape. The post-buckling behavior of perfect and imperfect, symmetric angle-ply, anti-symmetric angle-ply laminated resting on the tensionless Pasternak elastic foundation is obtained. The results showed that the unilateral constraint has an important influence on the post-buckling behavior at the stiffness of the foundation is sufficiently large.

(Shen and Xiang, 2019) [40] used the Two-Step perturbation approach to present the thermal post-buckling equilibrium paths of graphene-reinforced composite (GRC) laminated cylindrical shells. The structure was subjected to uniform temperature load with or without geometric imperfection. The governing equations of motion were derived by employing the Higher-Order Shear Deformation Shell Theory with Von-Karman type nonlinearity kinematic, a thermal effect also was included. The (GRC) layers were organized in (FG) graphene-reinforced arrangement with a different volume fraction of graphene in each (GRC) layer. The (GRC) shell can have snap or stability through the thermal equilibrium path of post-buckling under

a uniform field of temperature, depending on the shell geometric imperfection parameter and geometrical parameter. At the shell, under the uniform temperature field, the FG-X piece-wise FG graphene distribution can improve the capacity of a post-buckling of the shell.

2.5 SUMMARY OF LITERATURE REVIEW

Through the literature review, in the previous sections, many researchers focused on the study of buckling and post-buckling behavior under the influence of different mechanical subject to different boundary conditions.

Researchers examined the effect of the different parameters of the laminated composite plate on buckling behavior. With using different theories and methods are obtained the solution of the equations of motion [16-27].

In the second part of the literature review, researchers used different structures such as laminated plate, conical shell, and functionally graded plate. The equation motion is derived by used the FSDT and solved by employed several approaches like finite element (FEM), and the Ritz method as [28-32]. Then, in the last part of the literature review, other researchers investigated the behavior of stability for different structures by using the Two-Step perturbation technique with various theories to obtain the equilibrium equations [33-40].

In engineering applications, laminated composite plates are subjected to complex working conditions and severe types of static loads. Therefore these structures will be exposed for instability state that leads to buckling

phenomenon and failure. Thus, buckling and post-buckling research are important because it is one of the reasons for the failure of structures.

When the laminated composite plates are exposed to high compressive loads, these structures will fail. Thus, buckling and post-buckling research are important to avoid the instability of structures.

So far, by reviewing the previous researchers, and to the best authors' knowledge, there is no publication about non-linear static stability analyzed for the graphite/epoxy laminated composite plate under different mechanical loading (uniaxial load and biaxial load). Based on the first-order shear deformation theory plate with taking into consideration the geometrical nonlinearity in von Kármán sense, the equations of motion are determined. These equations are solved by applied the Two-Step perturbation technique method to obtain the critical buckling loads and post-buckling equilibrium paths.

CHAPTER THREE

BASIC FORMULATIONS

CHAPTER THREE

THEORETICAL FORMULATIONS AND MODELLING

3.1 INTRODUCTION

The aim of the current research is to study the effects of various compressive loads, and different parameters on the behavior of buckling and post-buckling of the laminated composite plate. The present model is subjected to compressive loads (uniaxial and biaxial). This will be achieved by finding the value of the critical buckling load, post-buckling equilibrium paths, and represent them on the loads-deflection scheme to discuss them in the next chapter.

In this chapter, the basic equations of motion for the nonlinear static stability behavior of laminated plates are derived based on first-order shear deformation theory. The certain assumption or restrictions in formulating this theory are as following (UnuthuReddy, 2003) [1]:

- ✓ The layers bonded together are perfect.
- ✓ The material of all layers is behaving elastically and has two planes of symmetrical material i.e., orthotropic material.
- ✓ The displacements and strains are as small compared with the thickness of the plate.

- ✓ The transverse shear stresses of the laminated on the top and bottom surfaces are zero therefore used shear correction factor in this theory.
- ✓ Each layer of the laminated plate is a uniform thickness.

These equations are solved by the two-step perturbation technique. Figure 3-1 illustrates the sequence of the analytical methods utilized to derive and solve the mathematical formulation for the current model.

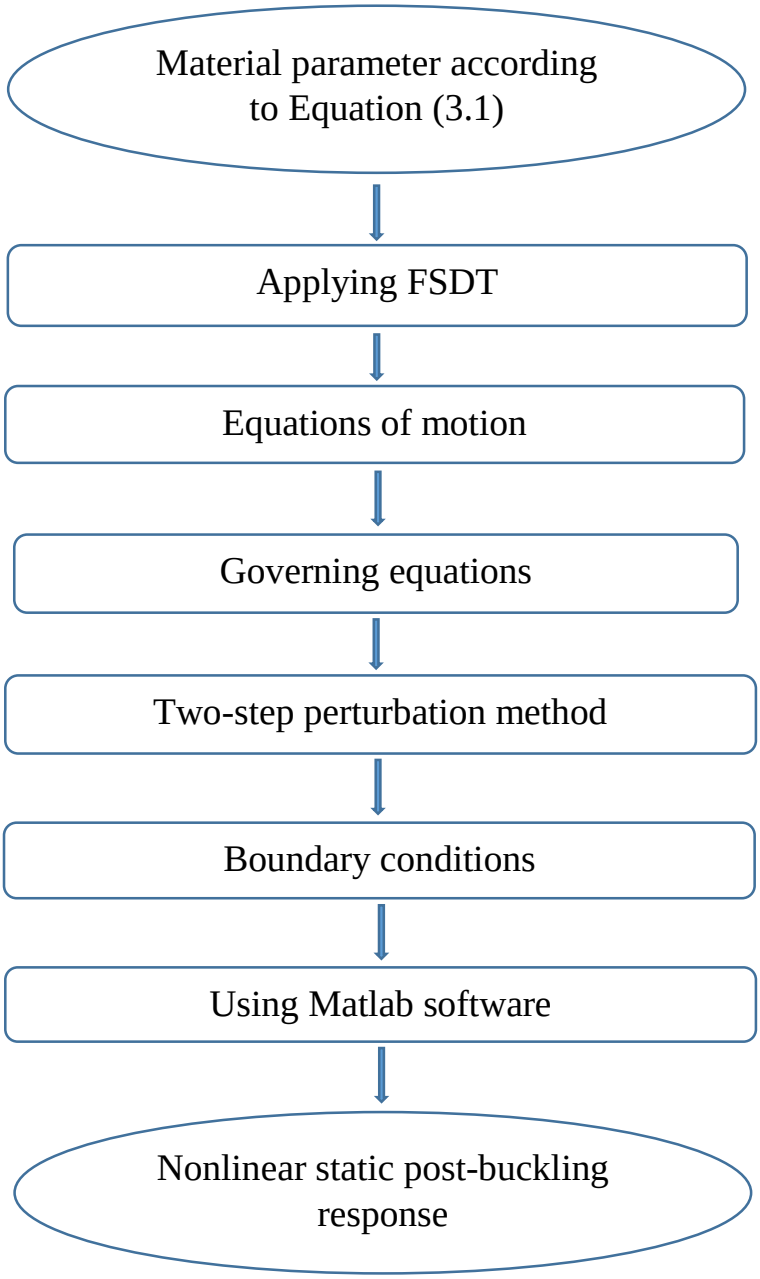

Figure 3-1: The sequence of preparation and analysis processes of the laminated composite plate model

3.2 GEOMETRIC MODEL

The geometry and coordinate of the composite plate model are shown in Figures 3-2 and 3-3, respectively, are unidirectional laminated plates of orthotropic materials. The symbols a, b, and h present the structure length, width, and thickness, respectively. The model is under uniformly distributed biaxial compression loads N_x and N_y along the edges $0 \leq x \leq a$ and $0 \leq y \leq b$, respectively. The symmetrically laminated plate was composed of number of layers (N) with equal thickness h / N, where N=10. The displacement parallels to the Cartesian Coordinates as axes x_1, y_2, are considered.

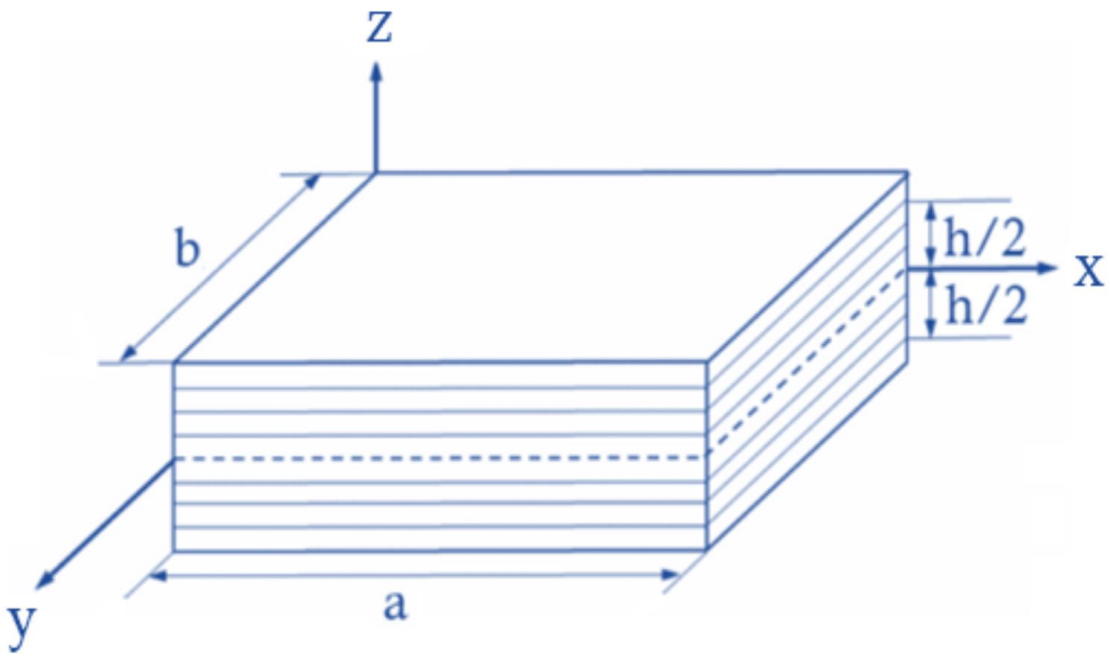

Figure 3-2: Geometry system of the laminated plate (Bhaskar and Thakur, 2019) [41].

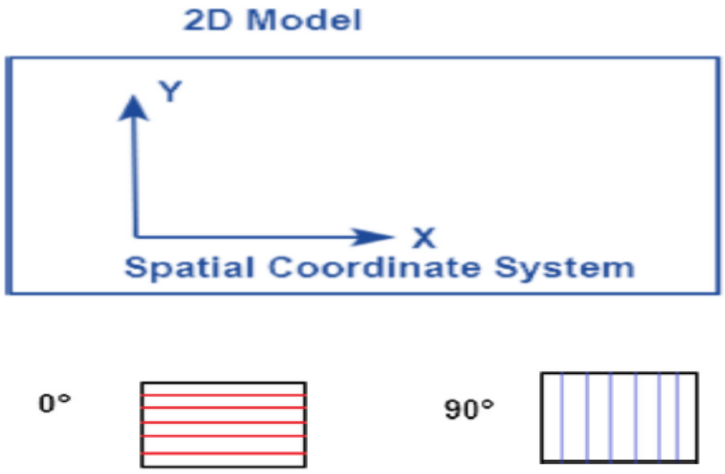

Figure 3-3: Coordinate of orthotropic materials (Li and Kim, 2020) [42].

3.3 MATERIAL PROPERTY

The lamina engineering constants, moduli, and Poisson's ratio of the fiber-reinforced material can be expressed as the follows (UnuthuReddy, 2003) [1]:

$$
\begin{aligned}
E_1 &= E_f\, V_f + E_m\, V_m \\
E_2 &= \frac{E_f E_m}{E_f V_m + E_m V_f} \\
v_{12} &= V_f v_f + V_m v_m \\
G_{12} &= \frac{G_f G_m}{G_f V_m + G_m V_f} \\
v_{21} &= \frac{v_{12}\, E_2}{E_1} \\
G_{23} &= G_{13} = G_{12}
\end{aligned}
\tag{3.1}
$$

where, E_1 and E_2 are the longitudinal and transverse modulus, respectively; v_{12} is the major Poisson's ratio, G_{12} , G_{13} , and G_{23} are the shear modulus which describes angular changes between the main directions respectively, x and y, x and z, y and z, respectively. Also:

E_f = Modulus of a fiber; E_m = Modulus of a matrix

v_f = Poisson's ratio of a fiber; v_m = Poisson's ratio of a matrix

V_f = Volume fraction of a fiber; V_m = Volume fraction of a matrix

$$G_f = \frac{E_f}{2(1+v_f)} \quad ; \quad G_m = \frac{E_m}{2(1+v_m)}$$

3.4 FORMULATION OF THE PROBLEM

3.4.1 DISPLACEMENT FIELD AND STRAINS

In this section, the equations of motion will be obtained by used the first-order shear deformation theory. By Ref.(Alieldin, Alshorbagy, and Shaat, 2011) [43], the displacement fields (u, v, ω) for laminated composite plates are assumed to be:

$$\begin{aligned} u(x,y,z) &= u_0(x,y) + z\phi_x(x,y) \\ v(x,y,z) &= v_0(x,y) + z\phi_y(x,y) \\ w(x,y,z) &= w_0(x,y) \end{aligned} \tag{3.2}$$

The (u_0, v_0, w_0) denotes the displacements of mid-plan at z=0. The ($\phi_x \; and \phi_y$) are the rotation of the transverse normal around the y_ and x_axes, respectively, as shown in Figure 3-4.

The quantities $(u_0, v_0, w_0, \phi_x, \phi_y)$ are unknown functions to be calculated. Note that $\phi_x = \frac{\partial u}{\partial z}$, $\phi_y = \frac{\partial v}{\partial z}$ as shown in Figure 3-4.

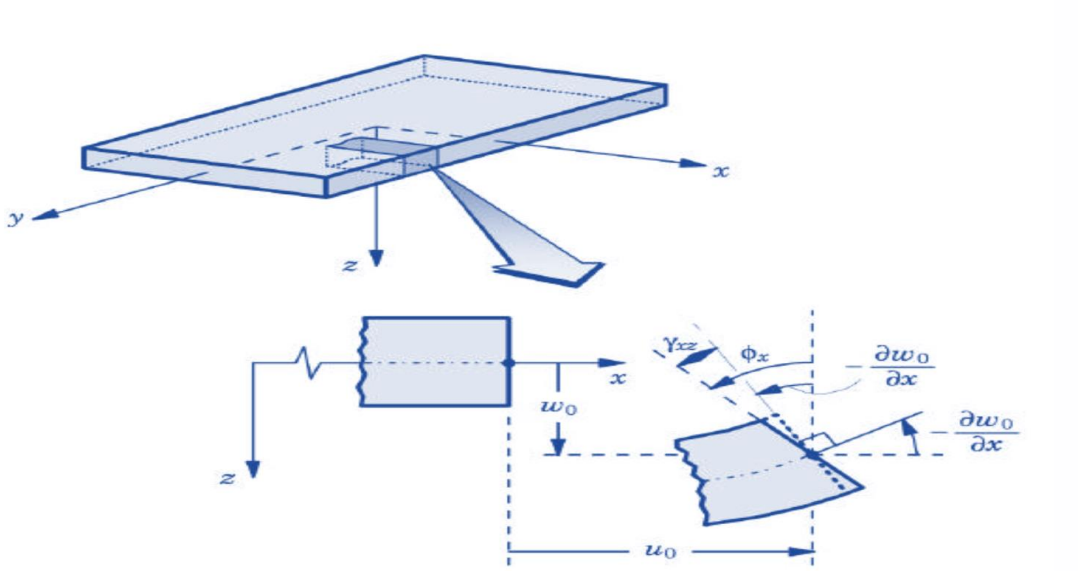

Figure 3-4: Undeformed and deformed geometries of an edge of a the plate under the assumptions of the FSDT (Alieldin, Alshorbagy, and Shaat, 2011) [43]

The strain-displacement relations for moderate rotations and small strains take the form (Ovesy and Kharazi, 2011) [44]:

$$\begin{aligned}
\varepsilon_x &= \frac{\partial u}{\partial x} + \frac{1}{2}\left(\frac{\partial w}{\partial x}\right)^2 \\
\varepsilon_y &= \frac{\partial v}{\partial y} + \frac{1}{2}\left(\frac{\partial w}{\partial y}\right)^2 \\
\varepsilon_{yz} &= \frac{1}{2}\left(\frac{\partial v}{\partial z} + \frac{\partial w}{\partial y}\right) \\
\varepsilon_{xz} &= \frac{1}{2}\left(\frac{\partial u}{\partial z} + \frac{\partial w}{\partial x}\right) \\
\varepsilon_{xy} &= \frac{1}{2}\left(\frac{\partial u}{\partial y} + \frac{\partial v}{\partial x} + \frac{\partial w}{\partial x}\frac{\partial w}{\partial y}\right) \\
\varepsilon_z &= \frac{\partial w}{\partial z}
\end{aligned} \tag{3.3}$$

By substituting equation (3.2) in equation (3.3), the Von Karman type nonlinear strains can be obtained as follows:

$$\varepsilon_x = \frac{\partial u_0}{\partial x} + \frac{1}{2}\left(\frac{\partial w_0}{\partial x}\right)^2 + z\frac{\partial \phi_x}{\partial x}$$

$$\varepsilon_y = \frac{\partial v_0}{\partial y} + \frac{1}{2}\left(\frac{\partial w_0}{\partial y}\right)^2 + z\frac{\partial \phi_y}{\partial y}$$

$$\gamma_{yz} = \frac{\partial w_0}{\partial y} + \phi_y \ , \quad \gamma_{xz} = \frac{\partial w_0}{\partial x} + \phi_x \tag{3.4}$$

$$\gamma_{xy} = \left(\frac{\partial u_0}{\partial y} + \frac{\partial v_0}{\partial x} + \frac{\partial w_0}{\partial x}\frac{\partial w_0}{\partial y}\right) + z\left(\frac{\partial \phi_x}{\partial y} + \frac{\partial \phi_y}{\partial x}\right)$$

$$\varepsilon_z = 0$$

Where $(\gamma_{yz}, \gamma_{xz}, \gamma_{xy})$ represent the transverse shear strains components in the planes (yz, xz, xy). The strains in equation (3.4) can be re-arranged in the form:

$$\begin{Bmatrix} \varepsilon_x \\ \varepsilon_y \\ \gamma_{yz} \\ \gamma_{xz} \\ \gamma_{xy} \end{Bmatrix} = \begin{Bmatrix} \varepsilon_x^{(0)} \\ \varepsilon_y^{(0)} \\ \gamma_{yz}^{(0)} \\ \gamma_{xz}^{(0)} \\ \gamma_{xy}^{(0)} \end{Bmatrix} + z\begin{Bmatrix} \varepsilon_x^{(1)} \\ \varepsilon_y^{(1)} \\ \gamma_{yz}^{(1)} \\ \gamma_{xz}^{(1)} \\ \gamma_{xy}^{(1)} \end{Bmatrix}$$

$$= \begin{Bmatrix} \frac{\partial u_0}{\partial x} + \frac{1}{2}\left(\frac{\partial w_0}{\partial x}\right)^2 \\ \frac{\partial v_0}{\partial y} + \frac{1}{2}\left(\frac{\partial w_0}{\partial y}\right)^2 \\ \phi_y + \frac{\partial w_0}{\partial y} \\ \phi_x + \frac{\partial w_0}{\partial x} \\ \frac{\partial u_0}{\partial y} + \frac{\partial v_0}{\partial x} + \frac{\partial w_0}{\partial x}\frac{\partial w_0}{\partial y} \end{Bmatrix} + z\begin{Bmatrix} \frac{\partial \phi_x}{\partial x} \\ \frac{\partial \phi_y}{\partial y} \\ 0 \\ 0 \\ \frac{\partial \phi_x}{\partial y} + \frac{\partial \phi_y}{\partial x} \end{Bmatrix} \tag{3.5}$$

3.4.2 STRESS-STRAIN RELATIONSHIPS

For a laminated composite plate, the nonlinear stress-strain relations can be written as follows (Roylance, 2000) [45].

$$\begin{Bmatrix}\sigma_1\\ \sigma_2\\ \tau_{12}\end{Bmatrix} = \begin{bmatrix} c^2 & s^2 & 2sc \\ s^2 & c^2 & -2sc \\ -sc & sc & c^2 - s^2 \end{bmatrix} \begin{Bmatrix}\sigma_x\\ \sigma_y\\ \tau_{xy}\end{Bmatrix} \tag{3.6}$$

Where c = cosθ, s = sinθ, and θ is the lay-up angle of reinforcement.

The equation (3.6) can be abbreviated as:

$$\sigma' = T\sigma \tag{3.7}$$

Where: T is the transformation matrix

Using mathematical, it can be shown that the components of infinitesimal strain transform by nearly the same relations:

$$\begin{Bmatrix}\varepsilon_1\\ \varepsilon_2\\ \frac{1}{2}\gamma_{12}\end{Bmatrix} = \mathrm{T}\begin{Bmatrix}\varepsilon_x\\ \varepsilon_y\\ \frac{1}{2}\gamma_{xy}\end{Bmatrix} \tag{3.8}$$

The factor 1/2 on the shear components arises from the classical definition of shear strain is twice the tensorial shear strain. By introducing Reuter's matrix, some discomfiture into the transformation relations can be reduced. Reuter's matrix is defined as:

$$[\mathrm{R}] = \begin{bmatrix}1 & 0 & 0\\ 0 & 1 & 0\\ 0 & 0 & 2\end{bmatrix} \quad \text{OR} \quad [\mathrm{R}]^{-1} = \begin{bmatrix}1 & 0 & 0\\ 0 & 1 & 0\\ 0 & 0 & \frac{1}{2}\end{bmatrix} \tag{3.9}$$

$$\begin{Bmatrix} \varepsilon_1 \\ \varepsilon_2 \\ \gamma_{12} \end{Bmatrix} = \mathrm{R} \begin{Bmatrix} \varepsilon_1 \\ \varepsilon_2 \\ \frac{1}{2}\gamma_{12} \end{Bmatrix} = RT \begin{Bmatrix} \varepsilon_1 \\ \varepsilon_2 \\ \frac{1}{2}\gamma_{12} \end{Bmatrix} = RT\mathrm{R}^{-1} \begin{Bmatrix} \varepsilon_x \\ \varepsilon_y \\ \gamma_{xy} \end{Bmatrix} \tag{3.10}$$

OR

$$\varepsilon' = \mathrm{RTR}^{-1}\varepsilon \tag{3.11}$$

Stress-strain relations of the orthotropic lamina are given below(Namdar and Darendeliler, 2017) [46]:

$$\begin{bmatrix} \sigma_1 \\ \sigma_2 \\ \tau_{12} \end{bmatrix} = \begin{bmatrix} Q_{11} & Q_{12} & 0 \\ Q_{12} & Q_{22} & 0 \\ 0 & 0 & Q_{66} \end{bmatrix} \begin{bmatrix} \varepsilon_1 \\ \varepsilon_2 \\ \gamma_{12} \end{bmatrix} \tag{3.12}$$

Coefficients of stiffness matrix can be obtained as:

$$\begin{aligned} Q_{11} &= \frac{E_1}{1 - v_{12}v_{21}} \quad ; \quad Q_{22} = \frac{E_2}{1 - v_{12}v_{21}} \\ Q_{12} &= \frac{v_{12}E_2}{1 - v_{12}v_{21}} = \frac{v_{21}E_1}{1 - v_{12}v_{21}} \quad ; \quad Q_{66} = G_{12} \end{aligned} \tag{3.13}$$

From substituting equation (3.12) in equation (3.6), it can be obtained:

$$\begin{Bmatrix} \sigma_x \\ \sigma_y \\ \tau_{xy} \end{Bmatrix} = \mathrm{T}^{-1} \begin{bmatrix} Q_{11} & Q_{12} & 0 \\ Q_{12} & Q_{22} & 0 \\ 0 & 0 & Q_{66} \end{bmatrix} \begin{bmatrix} \varepsilon_1 \\ \varepsilon_2 \\ \gamma_{12} \end{bmatrix} \tag{3.14}$$

By substituting equation (3.10) in equation (3.14), this gives the following expressions:

$$\begin{Bmatrix} \sigma_x \\ \sigma_y \\ \tau_{xy} \end{Bmatrix} = \mathrm{T}^{-1}\, Q\, \mathrm{RTR}^{-1} \begin{Bmatrix} \varepsilon_x \\ \varepsilon_y \\ \gamma_{xy} \end{Bmatrix} = \overline{Q} \begin{Bmatrix} \varepsilon_x \\ \varepsilon_y \\ \gamma_{xy} \end{Bmatrix} \tag{3.15}$$

Where, the term $\overline{Q} = \mathrm{T}^{-1}\, Q\, \mathrm{RTR}^{-1}$, is transformed reduced stiffness.

Substituting equation (3.5) in equation (3.15) gives the global stress for the laminate as:

$$\begin{Bmatrix}\sigma_x\\ \sigma_y\\ \tau_{xy}\end{Bmatrix}=\begin{bmatrix}\bar{Q}_{11} & \bar{Q}_{12} & 0\\ \bar{Q}_{12} & \bar{Q}_{22} & 0\\ 0 & 0 & \bar{Q}_{66}\end{bmatrix}^k\begin{Bmatrix}\varepsilon_x^{(0)}+z\varepsilon_x^{(1)}\\ \varepsilon_y^{(0)}+z\varepsilon_y^{(1)}\\ \varepsilon_{xy}^{(0)}+z\varepsilon_{xy}^{(1)}\end{Bmatrix} \tag{3.16}$$

Where:

$$\begin{aligned}\bar{Q}_{11} &= Q_{11}c^4+2(Q_{12}+2Q_{66})\,s^2\,c^2+Q_{22}s^4\\ \bar{Q}_{12} &= (Q_{11}+Q_{22}-4Q_{66})s^2c^2+Q_{12}(s^4+c^4)\\ \bar{Q}_{22} &= Q_{11}s^4\ \ +2(Q_{12}+2Q_{66})\,s^2\,c^2+Q_{22}c^4\\ \bar{Q}_{66} &= (Q_{11}+Q_{22}-2Q_{12}-2Q_{66})\,s^2\,c^2+Q_{66}(s^4+c^4)\end{aligned} \tag{3.17}$$

3.4.3 LAMINATE FORCE AND MOMENT RESULTANTS

Forces and moments that are applied onto a laminate can be obtained by integration of the stresses on each layer of the laminate plate through the thickness. The force and moments resultants for the kth layer of a laminated can be found as (Domfang, 2013) [47]:

$$\begin{aligned}N_x &= \sum_{k=1}^{NL}\int_{Z_k}^{Z_{k+1}}\sigma_x dz\\ N_y &= \sum_{k=1}^{NL}\int_{Z_k}^{Z_{k+1}}\sigma_y dz\\ N_{xy} &= \sum_{k=1}^{NL}\int_{Z_k}^{Z_{k+1}}\sigma_{xy} dz\end{aligned} \tag{3.18}$$

Where N_x and N_y were the normal force resultants, N_{xy} was the tangential force, NL was the number of layers.

$$M_x = \sum_{k=1}^{NL} \int_{Z_k}^{Z_{k+1}} z\sigma_x dz$$
$$M_y = \sum_{k=1}^{NL} \int_{Z_k}^{Z_{k+1}} z\sigma_y dz \qquad (3.19)$$
$$M_{xy} = \sum_{k=1}^{NL} \int_{Z_k}^{Z_{k+1}} z\sigma_{xy} dz$$

Where M_x and M_y were the moment resultants, and M_{xy} was the twisting moment.

By substituting equation (3.16) in equations (3.18) and (3.19), it can obtain the expressions:

$$\begin{Bmatrix} N_x \\ N_y \\ N_{xy} \end{Bmatrix} = \sum_{k=1}^{NL} \int_{Z_k}^{Z_{k+1}} \begin{bmatrix} \bar{Q}_{11} & \bar{Q}_{12} & 0 \\ \bar{Q}_{21} & \bar{Q}_{22} & 0 \\ 0 & 0 & \bar{Q}_{66} \end{bmatrix}^k \begin{Bmatrix} \varepsilon_x^{(0)} + z\varepsilon_x^{(1)} \\ \varepsilon_y^{(0)} + z\varepsilon_y^{(1)} \\ \varepsilon_{xy}^{(0)} + z\varepsilon_{xy}^{(1)} \end{Bmatrix} dz \qquad (3.20)$$

$$\begin{Bmatrix} M_x \\ M_y \\ M_{xy} \end{Bmatrix} = \sum_{k=1}^{NL} \int_{Z_k}^{Z_{k+1}} Z \begin{bmatrix} \bar{Q}_{11} & \bar{Q}_{12} & 0 \\ \bar{Q}_{21} & \bar{Q}_{22} & 0 \\ 0 & 0 & \bar{Q}_{66} \end{bmatrix}^k \begin{Bmatrix} \varepsilon_x^{(0)} + z\varepsilon_x^{(1)} \\ \varepsilon_y^{(0)} + z\varepsilon_y^{(1)} \\ \varepsilon_{xy}^{(0)} + z\varepsilon_{xy}^{(1)} \end{Bmatrix} dz \qquad (3.21)$$

Where, $\bar{Q}_{ij}$ are the lamina stiffness coefficients.

After integration equations (3.20) and (3.21), laminate constitutive equations are obtained as follows:

$$\begin{Bmatrix} N_x \\ N_y \\ N_{xy} \end{Bmatrix} = \begin{bmatrix} A_{11} & A_{12} & 0 \\ A_{12} & A_{22} & 0 \\ 0 & 0 & A_{66} \end{bmatrix} \begin{Bmatrix} \varepsilon_x^{(0)} \\ \varepsilon_y^{(0)} \\ \varepsilon_{xy}^{(0)} \end{Bmatrix} + \begin{bmatrix} B_{11} & B_{12} & 0 \\ B_{12} & B_{22} & 0 \\ 0 & 0 & B_{66} \end{bmatrix} \begin{Bmatrix} \varepsilon_x^{(1)} \\ \varepsilon_y^{(1)} \\ \varepsilon_{xy}^{(1)} \end{Bmatrix} \tag{3.22}$$

$$\begin{Bmatrix} M_x \\ M_y \\ M_{xy} \end{Bmatrix} = \begin{bmatrix} B_{11} & B_{12} & 0 \\ B_{12} & B_{22} & 0 \\ 0 & 0 & B_{66} \end{bmatrix} \begin{Bmatrix} \varepsilon_x^{(0)} \\ \varepsilon_y^{(0)} \\ \varepsilon_{xy}^{(0)} \end{Bmatrix} + \begin{bmatrix} D_{11} & D_{12} & 0 \\ D_{12} & D_{22} & 0 \\ 0 & 0 & D_{66} \end{bmatrix} \begin{Bmatrix} \varepsilon_x^{(1)} \\ \varepsilon_y^{(1)} \\ \varepsilon_{xy}^{(1)} \end{Bmatrix} \tag{3.23}$$

Where A_{ij} the extensional stiffness components, B_{ij} coupling stiffness components, and D_{ij} the bending stiffness components are defined as:

$$\begin{aligned} [A_{ij}] = \int_{-\frac{h}{2}}^{\frac{h}{2}} [\bar{Q}_{ij}]_k \, dz &= \sum_{k=1}^{NL} \int_{Z_k}^{Z_{k+1}} [\bar{Q}_{ij}]_k dz \\ &= \sum_{k=1}^{NL} [\bar{Q}_{ij}]_k (z_{k+1} - z_k) \end{aligned} \tag{3.24}$$

$$[B_{ij}] = \frac{1}{2} \sum_{k=1}^{NL} [\bar{Q}_{ij}]_k (z_{k+1}^2 - z_k^2) \tag{3.25}$$

$$[D_{ij}] = \frac{1}{3} \sum_{k=1}^{NL} [\bar{Q}_{ij}]_k (z_{k+1}^3 - z_k^3) \tag{3.26}$$

By using a compact form, Equations (3.22) and (3.23) can be written as below:

$$\begin{Bmatrix}\{N\}\\{M}\end{Bmatrix}=\begin{bmatrix}[A] & [B]\\ [B] & [D]\end{bmatrix}\begin{Bmatrix}\{\varepsilon^{(0)}\}\\{\varepsilon^{(1)}\}\end{Bmatrix} \tag{3.27}$$

Where, $\{\varepsilon^{(0)}\}$ and $\{\varepsilon^{(1)}\}$ are defined in equation (3.5).

Equation (3.27) can be presented in partial reverse forms with:

$$\begin{Bmatrix}\varepsilon^{(0)}\\M\end{Bmatrix}=\begin{bmatrix}\mathrm{A}^{*} & \mathrm{B}^{*}\\ -\mathrm{B}^{*} & \mathrm{D}^{*}\end{bmatrix}\begin{Bmatrix}\mathrm{N}\\\varepsilon^{(1)}\end{Bmatrix} \tag{3.28}$$

Where, $\mathrm{A}^{*}=\mathrm{A}^{-1}$, $\mathrm{B}^{*}=-\mathrm{A}^{-1}B$, and $\mathrm{D}^{*}=D-\mathrm{A}^{-1}B$.

For the cross-ply symmetric laminate composite plate the $[\mathrm{B}^{*}]$ should be zero.

The shear forces resultants Q_x and Q_y were expressed as:

$$\begin{Bmatrix}Q_y\\Q_x\end{Bmatrix}=\int_{-\frac{h}{2}}^{\frac{h}{2}}\begin{Bmatrix}\sigma_{yz}\\\sigma_{xz}\end{Bmatrix}dz \tag{3.29}$$

Augmented with:

$$\begin{Bmatrix}\sigma_{yz}\\\sigma_{xz}\end{Bmatrix}^{k}=\begin{bmatrix}\bar{Q}_{44} & 0\\ 0 & \bar{Q}_{55}\end{bmatrix}^{k}\begin{Bmatrix}\gamma_{yz}^{(0)}\\\gamma_{xz}^{(0)}\end{Bmatrix} \tag{3.30}$$

Substituting equation (3.30) in (3.29) was given:

$$\begin{Bmatrix}Q_y\\Q_x\end{Bmatrix}=K_s\begin{bmatrix}A_{44} & 0\\ 0 & A_{55}\end{bmatrix}\begin{Bmatrix}\gamma_{yz}^{(0)}\\\gamma_{xz}^{(0)}\end{Bmatrix} \tag{3.31}$$

Where K_s= 5/6, is the shear correction factor.

Also:

$$(A_{44}, A_{55}) = \int_{Z_k}^{Z_{k+1}} \left(\bar{Q}_{44}{}^{k}, \bar{Q}_{55}{}^{k} \right) dz$$
$$= \sum_{k=1}^{NL} \int_{Z_k}^{Z_{k+1}} \left(\bar{Q}_{44}{}^{k}, \bar{Q}_{55}{}^{k} \right) dz \qquad (3.32)$$
$$= \sum_{k=1}^{NL} \left(\bar{Q}_{44}{}^{k}, \bar{Q}_{55}{}^{k} \right) (z_{k+1} - z_k)$$

Where $\overline{Q}_{44} = Q_{44}\, c^2 + Q_{55}\, s^2$, $\bar{Q}_{55} = Q_{55}\, c^2 + Q_{44}\, s^2$, and $Q_{44} = G_{23}$, $Q_{55} = G_{13}$

With substituting equation (3.5) in equation (3.30) was obtained:

$$\begin{Bmatrix} Q_y \\ Q_x \end{Bmatrix} = K_s \begin{bmatrix} A_{44} & 0 \\ 0 & A_{55} \end{bmatrix} \begin{Bmatrix} \phi_y + \dfrac{\partial w_0}{\partial y} \\ \phi_x + \dfrac{\partial w_0}{\partial x} \end{Bmatrix} \qquad (3.33)$$

3.5 EQUATIONS OF MOTION

The minimum total potential energy of the orthotropic plate subjected to compressive loads is defined as (Javaheri and Eslami, 2002) [48]:

$$\prod = U = \frac{1}{2} \int \left(\sigma_x \varepsilon_x + \sigma_y \varepsilon_y + \sigma_{xy} \gamma_{xy} + \sigma_{xz} \gamma_{xz} + \sigma_{yz} \gamma_{yz} \right) dV \qquad (3.34)$$

Where, U is the strain energy of the plate based on first-order shear deformation theory.

The equilibrium equation of a structure can be obtained by the variational approach and can be written as:

$$\begin{aligned}\delta U = \int_0^b \int_0^a \int_{-\frac{h}{2}}^{\frac{h}{2}} \big(&\sigma_x \delta\varepsilon_x + \sigma_y \delta\varepsilon_y + \sigma_{xy}\delta\gamma_{xy} \\ &+ \sigma_{xz}\delta\gamma_{xz} \\ &+ \sigma_{yz}\delta\gamma_{yz}\big)\, dzdxdy\end{aligned} \tag{3.35}$$

Taking the variation of equation (3.5) as follows:

$$\begin{aligned}\delta\varepsilon_x &= \frac{\partial\delta u_0}{\partial X} + \frac{\partial w_0}{\partial X}\frac{\partial\delta w_0}{\partial X} + z\frac{\partial\delta\phi_x}{\partial X} \\ \delta\varepsilon_y &= \frac{\partial\delta v_0}{\partial Y} + \frac{\partial w_0}{\partial Y}\frac{\partial\delta w_0}{\partial Y} + z\frac{\partial\delta\phi_y}{\partial Y} \\ \delta\gamma_{xy} &= \frac{\partial\delta u_0}{\partial Y} + \frac{\partial\delta v_0}{\partial X} + \frac{\partial w_0}{\partial \mathrm{X}}\frac{\partial\delta w_0}{\partial Y} + \frac{\partial w_0}{\partial Y}\frac{\partial\delta w_0}{\partial X} + z\frac{\partial\delta\phi_x}{\partial Y} \\ &\quad + z\frac{\partial\delta\phi_y}{\partial X} \\ \delta\gamma_{xz} &= \frac{\partial\delta w_0}{\partial X} + \delta\phi_x \\ \delta\gamma_{yz} &= \frac{\partial\delta w_0}{\partial Y} + \delta\phi_y\end{aligned} \tag{3.36}$$

Substation equation (3.36) into equation (3.35) with taking into account the equations (3.18), (3.19), and (3.29). Then, integration that respects to (z) provides as:

$$\begin{aligned}\delta U = \int_0^b \int_0^a \Big[& N_x \left(\frac{\partial \delta u_0}{\partial X} + \frac{\partial w_0}{\partial X}\frac{\partial \delta w_0}{\partial X}\right) + M_x \frac{\partial \delta \phi_x}{\partial X} + \\ & M_y \frac{\partial \delta \phi_y}{\partial Y} + N_{xy}\left(\frac{\partial \delta u_0}{\partial Y} + \frac{\partial \delta v_0}{\partial X} + \frac{\partial w_0}{\partial X}\frac{\partial \delta w_0}{\partial Y} + \frac{\partial w_0}{\partial Y}\frac{\partial \delta w_0}{\partial X}\right) \\ & + M_{xy}\left(\frac{\partial \delta \phi_x}{\partial Y} + \frac{\partial \delta \phi_y}{\partial X}\right) + Q_x\left(\frac{\partial \delta w_0}{\partial X} + \delta \phi_x\right) \\ & + Q_y\left(\frac{\partial \delta w_0}{\partial Y} + \delta \phi_y\right)\Big] dxdy\end{aligned} \tag{3.37}$$

Now, the nonlinear motion equations of laminated composite plates based on first-order shear deformation theory can be derived by employing the integration by-part procedure as follows:

$$\delta u_0 : \frac{\partial N_x}{\partial X} + \frac{\partial N_{xy}}{\partial Y} = 0 \tag{3.38}$$

$$\delta v_0 : \frac{\partial N_{xy}}{\partial X} + \frac{\partial N_y}{\partial Y} = 0 \tag{3.39}$$

$$\begin{aligned}\delta w_0 : & \frac{\partial Q_x}{\partial X} + \frac{\partial Q_y}{\partial Y} + \frac{\partial}{\partial X}\left[N_x \frac{\partial w_0}{\partial X} + N_{xy}\frac{\partial w_0}{\partial Y}\right] \\ & + \frac{\partial}{\partial Y}\left[N_{xy}\frac{\partial w_0}{\partial X} + N_y \frac{\partial w_0}{\partial Y}\right] = 0\end{aligned} \tag{3.40}$$

$$\delta \phi_x : \frac{\partial M_x}{\partial X} + \frac{\partial M_{xy}}{\partial Y} - Q_x = 0 \tag{3.41}$$

$$\delta \phi_y : \frac{\partial M_{xy}}{\partial X} + \frac{\partial M_y}{\partial Y} - Q_y = 0 \tag{3.42}$$

Inserting equations (3.5) and (3.28) into equations (3.38)-(3.42), and then take into account the conditions of deformation compatibility of a plate, one can get:

$$\frac{\partial^2 \varepsilon_x^{(0)}}{\partial Y^2} + \frac{\partial^2 \varepsilon_y^{(0)}}{\partial X^2} - \frac{\partial^2 \gamma_{xy}^{(0)}}{\partial X\, \partial Y} = \left(\frac{\partial^2 w_0}{\partial X\, \partial Y}\right)^2 - \frac{\partial^2 w_0}{\partial X^2}\frac{\partial^2 w_0}{\partial Y^2} \tag{3.43}$$

The first two equations (3.38) and (3.39) are done automatically by applying the stress function as follows:

$$N_x = \frac{\partial^2 f}{\partial Y^2}\ , N_y = \frac{\partial^2 f}{\partial X^2}\ , N_{xy} = -\frac{\partial^2 f}{\partial X\, \partial Y} \tag{3.44}$$

Substituting equations (3.33), and (3.44) into equation (3.40), the non-linear stability equations are obtained as:

$$\begin{aligned} &K_s A_{55}\frac{\partial \phi_x}{\partial X} + K_s A_{55}\frac{\partial^2 w_0}{\partial X^2} + K_s A_{44}\frac{\partial \phi_y}{\partial Y} + K_s A_{44} \\ &\frac{\partial^2 w_0}{\partial Y^2} + \frac{\partial^2 f}{\partial Y^2}\frac{\partial^2 w_0}{\partial X^2} - 2\frac{\partial^2 f}{\partial X\, \partial Y}\frac{\partial^2 w_0}{\partial X\, \partial Y} + \frac{\partial^2 f}{\partial X^2}\frac{\partial^2 w_0}{\partial Y^2} = 0 \end{aligned} \tag{3.45}$$

Inserting equations 3.28 and 3.33 in equations (3.41) and (3.42) respectively, the non-linear stability equations are given as:

$$\begin{aligned} &D_{11}^* \frac{\partial^2 \phi_x}{\partial X^2} + D_{12}^* \frac{\partial^2 \phi_y}{\partial X\, \partial Y} + D_{66}^* \left(\frac{\partial^2 \phi_x}{\partial Y^2} + \frac{\partial^2 \phi_y}{\partial X\, \partial Y}\right) - K_s A_{55}\phi_x \\ &-K_s A_{55}\frac{\partial w_0}{\partial X} = 0 \end{aligned} \tag{3.46}$$

$$D_{66}^{*}\frac{\partial^2\phi_x}{\partial X\,\partial Y}+D_{66}^{*}\frac{\partial^2\phi_y}{\partial X^2}+D_{12}^{*}\frac{\partial\phi_x}{\partial X\,\partial Y}+D_{11}^{*}\frac{\partial^2\phi_y}{\partial Y^2}-K_s\,A_{44}\phi_y-K_s\,A_{44}\frac{\partial w_0}{\partial Y}=0 \tag{3.47}$$

By inserting equations (3.28) and (3.44) in equation (3.43) the non-linear compatibility equation can be accomplished as gives:

$$A_{11}^{*}\frac{\partial^4 f}{\partial Y^4}+A_{11}^{*}\frac{\partial^4 f}{\partial X^4}+\left(A_{66}^{*}-2A_{12}^{*}\right)\frac{\partial^4 f}{\partial X^2\,\partial Y^2}=\left(\frac{\partial^2 w_0}{\partial X\,\partial Y}\right)^2-\frac{\partial^2 w_0}{\partial X^2}\frac{\partial^2 w_0}{\partial Y^2} \tag{3.48}$$

3.6 GOVERNING EQUATIONS

Introducing the following dimensionless quantities (Song et al., 2017) [33]:

$$x=\pi\frac{X}{a},y=\pi\frac{Y}{b},\beta=\frac{a}{b},\Delta=(D_{11}^{*}D_{22}^{*}A_{11}^{*}A_{22}^{*})^{\frac{1}{4}}$$
$$W_0=\frac{w_0}{\Delta},\qquad F=\frac{f}{(D_{11}^{*}D_{22}^{*})^{\frac{1}{2}}},\left(\bar{\phi}_x,\bar{\phi}_y\right)=\frac{a}{\pi}\frac{\left(\phi_x,\phi_y\right)}{\Delta} \tag{3.49}$$
$$\left(\lambda_{x,}\lambda_y\right)=\frac{\left(N_x b\,,N_y a\right)}{4\pi^2(D_{11}^{*}D_{22}^{*})^{\frac{1}{2}}}$$

Where $A_{22}^{*}=A_{11}^{*}$, $D_{22}^{*}=D_{11}^{*}$.

By inserting equation (3.49) in (3.45) and dividing byΔ, $\frac{\pi^2}{a^2}$, and D_{11}^{*}, and then multiplying by $\frac{a^2}{\pi^2}$, leads:

$$\gamma_{11}\frac{\partial^2 W_0}{\partial x^2}+\gamma_{12}\frac{\partial^2 W_0}{\partial y^2}+\gamma_{13}\frac{\partial\bar{\phi}_x}{\partial x}+\gamma_{14}\frac{\partial\bar{\phi}_y}{\partial y}+\beta^2 L(W_0,F)=0 \tag{3.50}$$

By inserting equation (3.49) in (3.46) and (3.47), then dividing by D_{11}^{*} and $\frac{\pi^2}{a^2}$, leads:

$$\gamma_{15}\frac{\partial W_0}{\partial x}+\frac{\partial^2\bar{\phi}_x}{\partial x^2}+\gamma_{16}\frac{\partial^2\bar{\phi}_x}{\partial y^2}+\gamma_{17}\bar{\phi}_x+\gamma_{18}\frac{\partial^2\bar{\phi}_y}{\partial x\,\partial y}=0 \qquad (3.51)$$

$$\gamma_{19}\frac{\partial W_0}{\partial y}+\gamma_{20}\frac{\partial^2\bar{\phi}_y}{\partial x^2}+\gamma_{21}\frac{\partial^2\bar{\phi}_y}{\partial y^2}+\gamma_{22}\bar{\phi}_y+\gamma_{23}\frac{\partial^2\bar{\phi}_x}{\partial x\,\partial y}=0 \qquad (3.52)$$

By inserting equation (3.49) in (3.48), then dividing by $A_{11}^{*}(D_{11}^{*}D_{22}^{*})^{\frac{1}{2}}\frac{\pi^4}{a^4}$ leads:

$$\frac{\partial^4 F}{\partial x^4}+\gamma_{24}\frac{\partial^4 F}{\partial x^2\,\partial y^2}+\gamma_{25}\frac{\partial^4 F}{\partial y^4}=-\frac{1}{2}\beta^2 L(W_0,W_0) \qquad (3.53)$$

Where γ_{ij} are detailed in Appendix A, and a nonlinear partial differential operator $L(\,)=\frac{\partial^2}{\partial x^2}\frac{\partial^2}{\partial y^2}-2\frac{\partial^2}{\partial x\,\partial y}\frac{\partial^2}{\partial x\,\partial y}+\frac{\partial^2}{\partial y^2}\frac{\partial^2}{\partial x^2}$.

The governing equations (3.50) - (3.53) respectively, can be written in terms of W_0,$\bar{\phi}_x$, $\bar{\phi}_y$ and F as follows:

$$L_{01}(W_0)+L_{02}(\bar{\phi}_x)+L_{03}(\bar{\phi}_y)+\beta^2 L(W_0,F)=0 \qquad (3.54)$$

$$L_{04}(W_0)+L_{05}(\bar{\phi}_x)+L_{06}(\bar{\phi}_y)=0 \qquad (3.55)$$

$$L_{07}(W_0)+L_{08}(\bar{\phi}_x)+L_{09}(\bar{\phi}_y)=0 \qquad (3.56)$$

$$L_{10}(F)=-\frac{1}{2}\beta^2 L(W_0,W_0) \qquad (3.57)$$

Where L_{ij} is given in Appendix A and represents the linear partial differential operator.

3.7 BOUNDARY CONDITIONS

The boundary conditions for the laminated composite plate simply supported on all edges are (Song et al.2017) [33]:

$x = 0, \pi$:

$$\bar{\phi}_y = W_0 = 0 \tag{3.58}$$

$$M_x = \frac{\partial^2 F}{\partial x \, \partial y} = 0 \tag{3.59}$$

$$4\lambda_x + \frac{1}{\pi}\int_0^{\pi} \frac{\partial^2 F}{\partial y^2}\,\mathrm{d}y = 0 \tag{3.60}$$

$y = 0, \pi$:

$$\bar{\phi}_x = W_0 = 0 \tag{3.61}$$

$$M_y = \frac{\partial^2 F}{\partial x \, \partial y} = 0 \tag{3.62}$$

$$4\lambda_y + \frac{1}{\pi}\int_0^{\pi} \frac{\partial^2 F}{\partial x^2}\,\mathrm{d}x = 0 \tag{3.63}$$

3.8 ANALYTICAL APPROACH AND ASYMPTOTIC SOLUTIONS

The two-step perturbation method is employed to solve equations (3.50)-(3.53) to examine the critical buckling loads and post-buckling equilibrium laminated composite plates. The solutions of equations (3.50)-(3.53) are supposed to take the form of (Shen, 2013) [15]:

$$W_0(x,y,\varepsilon)=\sum_{j=1}\varepsilon^j\bar{w}_{0j}\,(x,y),F(x,y,\varepsilon)=\sum_{j=0}\varepsilon^j\bar{f}_j(x,y)$$
$$\bar{\phi}_x(x,y,\varepsilon)=\sum_{j=1}\varepsilon^j\varphi_{xj}(x,y),\bar{\phi}_y(x,y,\varepsilon)=\sum_{j=1}\varepsilon^j\varphi_{yj}(x,y) \quad (3.64)$$

Where ε : is the small perturbation parameter.

By substituting equation (3.64) into equations (3.54) - (3.57) respectively, yields:

$$L_{01}(\varepsilon^1\bar{w}_{01}+\varepsilon^2\bar{w}_{02}+\varepsilon^3\bar{w}_{03}+\varepsilon^4\bar{w}_{04})+L_{02}(\varepsilon^1\varphi_{x1}+\varepsilon^2\varphi_{x2}+\varepsilon^3\varphi_{x3}+\varepsilon^4\varphi_{x4})+L_{03}(\varepsilon^1\varphi_{y1}+\varepsilon^2\varphi_{y2}+\varepsilon^3\varphi_{y3}+\varepsilon^4\varphi_{y4})+\beta^2L(\varepsilon^1\bar{w}_{01}+\varepsilon^2\bar{w}_{02}+\varepsilon^3\bar{w}_{03}+\varepsilon^4\bar{w}_{04})(\varepsilon^0\bar{f}_0+\varepsilon^1\bar{f}_1+\varepsilon^2\bar{f}_2+\varepsilon^3\bar{f}_3+\varepsilon^4\bar{f}_4)=0 \quad (3.65)$$

$$L_{04}(\varepsilon^1\bar{w}_{01}+\varepsilon^2\bar{w}_{02}+\varepsilon^3\bar{w}_{03}+\varepsilon^4\bar{w}_{04})+L_{05}(\varepsilon^1\varphi_{x1}+\varepsilon^2\varphi_{x2}+\varepsilon^3\varphi_{x3}+\varepsilon^4\varphi_{x4})+L_{06}(\varepsilon^1\varphi_{y1}+\varepsilon^2\varphi_{y2}+\varepsilon^3\varphi_{y3}+\varepsilon^4\varphi_{y4})=0 \quad (3.66)$$

$$L_{07}(\varepsilon^1\bar{w}_{01}+\varepsilon^2\bar{w}_{02}+\varepsilon^3\bar{w}_{03}+\varepsilon^4\bar{w}_{04})+L_{08}(\varepsilon^1\varphi_{x1}+\varepsilon^2\varphi_{x2}+\varepsilon^3\varphi_{x3}+\varepsilon^4\varphi_{x4})+L_{09}(\varepsilon^1\varphi_{y1}+\varepsilon^2\varphi_{y2}+\varepsilon^3\varphi_{y3}+\varepsilon^4\varphi_{y4})=0 \quad (3.67)$$

$$L_{10}\ (\varepsilon^0\bar{f}_0\ +\ \varepsilon^1\bar{f}_1\ +\varepsilon^2\bar{f}_2\ +\varepsilon^3\bar{f}_3\ +\ \varepsilon^4\bar{f}_4\ ) = -\frac{1}{2}\beta^2 L$$
$$(\varepsilon^1\overline{w}_{01}\ +\ \varepsilon^2\overline{w}_{02}\ +\varepsilon^3\overline{w}_{03}\ +\varepsilon^4\overline{w}_{04}\ )\ (\varepsilon^1\overline{w}_{01}\ +\ \varepsilon^2\overline{w}_{02}\ + \tag{3.68}$$
$$\varepsilon^3\overline{w}_{03}\ +\varepsilon^4\overline{w}_{04}\ )$$

By determining the terms of equations (3.65) – (3.68) of the same order of ε. $\overline{w}_{0j}$, φ_{xj} , $\bar{f}_j$ and φ_{yj} are independent of ε, which can be setting the coefficient of each power of perturbation parameter (ε) equal to zero, this yields to the following set of equations:

Order ε^0 :

$$L_{10}(\bar{f}_0) = 0 \tag{3.69}$$

The solution of equation (3.65) is easy to be expressed by:

$$\bar{f}_o = -B_{00}^{(0)}\frac{y^2}{2} - b_{00}^{(0)}\frac{x^2}{2} \tag{3.70}$$

Order ε^1 :

$$L_{01}(\overline{w}_{01}) + L_{02}(\varphi_{x1}) + L_{03}(\varphi_{y1}) + \beta^2 L(\overline{w}_{01}, \bar{f}_0) = 0 \tag{3.71}$$

$$L_{04}(\overline{w}_{01}) + L_{05}(\varphi_{x1}) + L_{06}(\varphi_{y1}) = 0 \tag{3.72}$$

$$L_{07}(\overline{w}_{01}) + L_{08}(\varphi_{x1}) + L_{09}(\varphi_{y1}) = 0 \tag{3.73}$$

$$L_{10}(\bar{f}_1) = 0 \tag{3.74}$$

It is assumed that the solutions of equations (3.71) - (3.74) satisfying the simply supported boundary conditions have the form:

$$\overline{w}_{01}(x,y) = A_{11}^{(1)} \sin mx \sin ny \tag{3.75}$$

$$\varphi_{x1} = \varepsilon C_{11}^{(1)} \cos mx \sin ny \tag{3.76}$$

$$\phi_{y1} = \varepsilon D_{11}^{(1)} \sin mx \cos ny \tag{3.77}$$

$$\bar{f}_1 = 0 \tag{3.78}$$

Substituting equation (3.70), (3.75), (3.76), (3.77), and (3.78) into equations (3.71) – (3.74) yields:

$$\begin{aligned}\beta^2 A_{11}^{(1)}\left(b_{00}^{(0)} n^2 + B_{00}^{(0)} m^2\right) = (\gamma_{11} m^2 + \gamma_{12} n^2) A_{11}^{(1)} \\ + m\gamma_{13} C_{11}^{(1)} + n\gamma_{14} D_{11}^{(1)}\end{aligned} \tag{3.79}$$

Where:

$$C_{11}^{(1)} = \frac{r_{11}^{C}}{r_{11}} A_{11}^{(1)}, D_{11}^{(1)} = \frac{r_{11}^{D}}{r_{11}} A_{11}^{(1)} \tag{3.80}$$

In which, the coefficients in equations (3.80) are given in Appendix B.

Order ε^2:

$$\begin{aligned}&L_{01}(\overline{w}_{02}) + L_{02}(\varphi_{x2}) + L_{03}\left(\varphi_{y2}\right) + \beta^2 L(w_{02}, f_0) \\ &+\beta^2 L\left(\overline{w}_{01}, \bar{f}_1\right) = 0\end{aligned} \tag{3.81}$$

$$L_{04}(\overline{w}_{02}) + L_{05}(\varphi_{x2}) + L_{06}\left(\varphi_{y2}\right) = 0 \tag{3.82}$$

$$L_{07}(\overline{w}_{02}) + L_{08}(\varphi_{x2}) + L_{09}\left(\varphi_{y2}\right) = 0 \tag{3.83}$$

$$L_{10}\left(\bar{f}_2\right) = -\frac{1}{2}\beta^2 L(\overline{w}_{01}, \overline{w}_{01}) \tag{3.84}$$

It is assumed that the solutions of equations (3.81) - (3.84) satisfying the simply supported boundary conditions have the form:

$$\bar{w}_{02} = 0 \tag{3.85}$$

$$\varphi_{x2} = 0 \tag{3.86}$$

$$\varphi_{y2} = 0 \tag{3.87}$$

$$\bar{f}_2 = -b_{00}^{(2)} \frac{x^2}{2} - B_{00}^{(2)} \frac{y^2}{2} + B_{20}^{(2)} \cos 2mx + B_{02}^{(2)} \cos 2ny \tag{3.88}$$

The solution of equation (3.88) comes from the right-hand side of equation (3.84), and it is not necessary to guess it.

By substituting equation (3.88) into equation (3.84), one has:

$$B_{20}^{(2)} = \frac{\beta^2 n^2}{32m^2} A_{11}^{(1)2} \tag{3.89}$$

$$B_{02}^{(2)} = \frac{\beta^2 m^2}{32n^2 \gamma_{25}} A_{11}^{(1)2} \tag{3.90}$$

Order ε^3

$$L_{01}(\bar{w}_{03}) + L_{02}(\varphi_{x3}) + L_{03}(\varphi_{y3}) + \beta^2 L(\bar{w}_{03}, \bar{f}_0) + \beta^2 L(\bar{w}_{02}, \bar{f}_0) + \beta^2 L(\bar{w}_{01}, \bar{f}_2) = 0 \tag{3.91}$$

$$L_{04}(\bar{w}_{03}) + L_{05}(\varphi_{x3}) + L_{06}(\varphi_{y3}) = 0 \tag{3.92}$$

$$L_{07}(\bar{w}_{03}) + L_{08}(\varphi_{x3}) + L_{09}(\varphi_{y3}) = 0 \tag{3.93}$$

$$L_{10}(\bar{f}_3) = -\frac{1}{2}\beta^2 L(\bar{w}_{01}, \bar{w}_{02}) - \frac{1}{2}\beta^2 L(\bar{w}_{02}, \bar{w}_{01}) \tag{3.94}$$

It is assumed that the solutions of equations (3.91) - (3.94) satisfying the simply supported boundary conditions have the form:

$$\overline{w}_{03} = A_{13}^{(3)}\sin mx\,\sin 3ny + A_{31}^{(3)}\sin 3mx\,\sin ny \tag{3.95}$$

$$\varphi_{x3} = C_{13}^{(3)}\cos mx\,\sin 3ny + C_{31}^{(3)}\cos 3mx\,\sin ny \tag{3.96}$$

$$\varphi_{y3} = D_{13}^{(3)}\sin mx\,\cos 3ny + D_{31}^{(3)}\sin 3mx\,\cos ny \tag{3.97}$$

$$\bar{f}_3 = 0 \tag{3.98}$$

Substituting equations (3.69), (3.75), (3.85), (3.88), (3.95), (3.96), (3.97), and (3.98) into equations (3.91) – (3.94) yields:

$$m^2 B_{00}^{(2)} + n^2 b_{00}^{(2)} = 2m^2 n^2\left(B_{02}^{(2)} + B_{20}^{(2)}\right) \tag{3.99}$$

$$A_{13}^{(3)} = \frac{r_{13}^{A}}{r_{13}} A_{11}^{(1)3} \tag{3.100}$$

$$C_{13}^{(3)} = \frac{r_{13}^{C}}{r_{13}} A_{11}^{(1)3} \tag{3.101}$$

$$D_{13}^{(3)} = \frac{r_{13}^{D}}{r_{13}} A_{11}^{(1)3} \tag{3.102}$$

$$A_{31}^{(3)} = \frac{r_{31}^{A}}{r_{31}} A_{11}^{(1)3} \tag{3.103}$$

$$C_{31}^{(3)} = \frac{r_{31}^{C}}{r_{31}} A_{11}^{(1)3} \tag{3.104}$$

$$D_{31}^{(3)} = \frac{r_{31}^{D}}{r_{31}} A_{11}^{(1)3} \tag{3.105}$$

In which, Coefficients in Equations (3.100) – (3.105) are given in Appendix B.

Order ε^4

$$L_{01}(\overline{w}_{04}) + L_{02}(\varphi_{x4}) + L_{03}(\varphi_{y4}) + \beta^2 L(w_{04}, f_0) + \beta^2 L(\overline{w}_{03}, f_1) + \beta^2 L(\overline{w}_{02}, f_2) + \beta^2 L(w_1, f_3) = 0 \quad (3.106)$$

$$L_{04}(w_4) + L_{05}(\varphi_{x4}) + L_{06}(\varphi_{y4}) = 0 \quad (3.107)$$

$$L_{07}(w_4) + L_{08}(\varphi_{x4}) + L_{09}(\varphi_{y4}) = 0 \quad (3.108)$$

$$L_{10}(\bar{f}_4) = -\frac{1}{2}\beta^2 L(\overline{w}_{01}, \overline{w}_{03}) - \frac{1}{2}\beta^2 L(\overline{w}_{02}, \overline{w}_{02}) - \frac{1}{2}\beta^2 L(\overline{w}_{03}, \overline{w}_{01}) \quad (3.109)$$

It is assumed that the solutions of equations (3.106) - (3.109) satisfying the simply supported boundary conditions have the form:

$$\overline{w}_{04} = 0 \quad (3.110)$$

$$\varphi_{x4} = 0 \quad (3.111)$$

$$\varphi_{y4} = 0 \quad (3.112)$$

$$\bar{f}_4 = (-b_{00}^{(4)}\frac{x^2}{2} - B_{00}^{(4)}\frac{y^2}{2} + B_{20}^{(4)}\cos 2mx + B_{02}^{(4)}\cos 2ny + B_{40}^{(4)}\cos 4mx + B_{04}^{(4)}\cos 4ny + B_{24}^{(4)}\cos 2mx \cos 4ny + B_{42}^{(4)}\cos 4mx \cos 2ny) \quad (3.113)$$

Substituting equations (3.113) into equations (3.109) yields:

$$\begin{aligned}\left(m^2B_{00}^{(4)}+n^2b_{00}^{(4)}\right)\beta^2A_{11}^{(1)}=2\left(B_{02}^{(4)}+B_{20}^{(4)}\right)m^2n^2\beta^2A_{11}^{(1)}\\-2\left(A_{13}^{(3)}B_{02}^{(2)}+A_{31}^{(3)}B_{20}^{(2)}\right)m^2n^2\beta^2\end{aligned}\tag{3.114}$$

$$B_{20}^{(4)}=-\frac{r_{31}^{A}}{r_{31}}\frac{\beta^2n^2}{16m^2}A_{11}^{(1)4}\tag{3.115}$$

$$B_{02}^{(4)}=-\frac{r_{13}^{A}}{r_{13}}\frac{\beta^2m^2}{16\gamma_{25}n^2}A_{11}^{(1)4}\tag{3.116}$$

$$B_{22}^{(4)}=\frac{\beta^2m^2n^2}{4(m^4+\gamma_{24}m^2n^2+\gamma_{25}n^4)}\left(\frac{r_{13}^{A}}{r_{13}}+\frac{r_{31}^{A}}{r_{31}}\right)A_{11}^{(1)4}\tag{3.117}$$

$$B_{42}^{(4)}=-\frac{\beta^2m^2n^2}{256m^4+64\gamma_{24}m^2n^2+16\gamma_{25}n^4}\frac{r_{31}^{A}}{r_{31}}A_{11}^{(1)4}\tag{3.118}$$

$$B_{24}^{(4)}=-\frac{\beta^2m^2n^2}{16m^4+64\gamma_{24}m^2n^2+256\gamma_{25}n^4}\frac{r_{13}^{A}}{r_{13}}A_{11}^{(1)4}\tag{3.119}$$

$$B_{40}^{(4)}=\frac{\beta^2n^2}{64m^2}\frac{r_{31}^{A}}{r_{31}}A_{11}^{(1)4}\tag{3.120}$$

$$B_{04}^{(4)}=\frac{\beta^2m^2n^2}{64\gamma_{25}}\frac{r_{13}^{A}}{r_{13}}A_{11}^{(1)4}\tag{3.121}$$

In which, the coefficients in Equations (3.114) – (3.121) are given in Appendix B.

The asymptotic solutions of the displacement and stress function of the laminated plate are constructed as:

$$\begin{aligned}W_0=\varepsilon A_{11}^{(1)}\sin mx\sin ny+\varepsilon^3(A_{13}^{(3)}\sin mx\sin 3ny\\+A_{31}^{(3)}\sin 3mx\sin ny)\end{aligned}\tag{3.122}$$

$$\begin{aligned}\bar{\phi}_x=\varepsilon C_{11}^{(1)}\cos mx\sin ny+\varepsilon^3(C_{13}^{(3)}\cos mx\sin 3ny\\+C_{31}^{(3)}\cos 3mx\sin ny)\end{aligned}\tag{3.123}$$

$$\bar{\phi}_y = \varepsilon D_{11}^{(1)} \sin mx \cos ny + \varepsilon^3 (D_{13}^{(3)} \sin mx \cos 3ny + D_{31}^{(3)} \sin 3mx \cos ny) \tag{3.124}$$

$$\begin{aligned} F = & -b_{00}^{(0)} \frac{x^2}{2} - B_{00}^{(0)} \frac{y^2}{2} + \varepsilon^2 (-b_{00}^{(2)} \frac{x^2}{2} - B_{00}^{(2)} \frac{y^2}{2} \\ & + B_{20}^{(2)} \cos 2mx + B_{02}^{(2)} \cos 2ny) + \varepsilon^4 (-b_{00}^{(4)} \frac{x^2}{2} \\ & - B_{00}^{(4)} \frac{y^2}{2} + B_{20}^{(4)} \cos 2mx + B_{02}^{(4)} \cos 2ny \\ & + B_{22}^{(4)} \cos 2mx \cos 2ny + B_{40}^{(4)} \cos 4mx \\ & + B_{04}^{(4)} \cos 4ny + B_{24}^{(4)} \cos 2mx \cos 4ny \\ & + B_{42}^{(4)} \cos 4mx \cos 2ny) \end{aligned} \tag{3.125}$$

3.9 BUCKLING AND POSTBUCKLING

The post-buckling equilibrium paths of the laminated plate under biaxial compressive loads can be obtained by substituting equations (3.125) into equations (3.60) and (3.63) as follows:

$$4\lambda_x = B_{00}^{(0)} + \varepsilon^2 B_{00}^{(2)} + \varepsilon^4 B_{00}^{(4)} \tag{3.126}$$

$$4\lambda_y = b_{00}^{(0)} + \varepsilon^2 b_{00}^{(2)} + \varepsilon^4 b_{00}^{(4)} \tag{3.127}$$

By taking $(x, y) = (\pi / 2m, \pi / 2n)$ at m=n=1, W_{0m} the dimensionless maximum deflection can be obtained from equation (3.122):

$$W_{0m} = \varepsilon A_{11}^{(1)} - \varepsilon^3 \left(A_{13}^{(3)} + A_{31}^{(3)}\right) \tag{3.128}$$

Inversely, one has:

$$\varepsilon A_{11}^{(1)} = W_{0m} + \left(\frac{r_{13}^A}{r_{13}} + \frac{r_{31}^A}{r_{31}}\right) {W_{0m}}^3 \tag{3.129}$$

Where $r_{13}, r_{31}, r_{13,}^A$ and r_{31}^A are given in Appendix B, $\varepsilon A_{11}^{(1)}$ perturbation parameter, and ${W_{0m}}^3 = \varepsilon^3 A_{11}^{(3)}$.

With multiplying equation (3.126) and (3.127) by m^2 and n^2 respectively, utilizing the relations in equations (3.79), (3.99), and (3.114) then replacing $\varepsilon A_{11}^{(1)}$ with W_{0m} , that can be given:

$$\begin{aligned} 4\lambda_x m^2 + 4\lambda_y n^2 = {} & \frac{r_{11}\gamma_{11}m^2 + r_{11}\gamma_{12}n^2}{r_{11}\beta^2} \\ & + \frac{m\gamma_{13}r_{11}^C + n\gamma_{14}r_{11}^D}{r_{11}\beta^2} + \beta^2\left(\frac{m^4}{16\gamma_{25}} + \frac{n^4}{16}\right){W_{0m}}^2 - \\ & \left[\left(\frac{r_{31}^A}{r_{31}}\frac{n^4}{8} + \frac{r_{13}^A}{r_{13}}\frac{m^4}{8\gamma_{25}}\right)\beta^2 + \left(\begin{array}{c}\frac{r_{13}^A}{r_{13}}\frac{m^2}{16n^2\gamma_{25}} \\ + \frac{r_{31}^A}{r_{31}}\frac{n^2}{16m^2}\end{array}\right)\right]{W_{0m}}^4 \end{aligned} \tag{3.130}$$

By setting W_{0m} = 0 in equation (3.130), it can be simplified as:

$$\begin{aligned} 4r_{11}\beta^2\left(\lambda_x m^2 + \lambda_y n^2\right) = {} & r_{11}\gamma_{11}m^2 + r_{11}\gamma_{12}n^2 \\ & + m\gamma_{13}r_{11}^C + n\gamma_{14}r_{11}^D \end{aligned} \tag{3.131}$$

This formula is known as the analysis of linear buckling of a laminated plate under biaxial compressive loads.

Usually, p_x and p_y, the compressive load, vary proportionally, also $\sigma_y = \alpha\sigma_y$ where α is a constant, hence:

$$\alpha = \frac{\lambda_y}{\beta^2 \lambda_x} \tag{3.132}$$

With substituting Equation (3.132) into Equation (3.130) can be obtained post-buckling equilibrium paths of the laminated composite plate in terms of a non-dimensional maximum deflection W_{0m} as follows:

$$\lambda_x = \lambda_x^{(0)} + \lambda_x^{(2)} {W_{0m}}^2 + \lambda_x^{(4)} {W_{0m}}^4 \tag{3.133}$$

Where the post-buckling coefficients are given as:

$$\lambda_x^{(0)} = \frac{r_{11}\gamma_{11}m^2 + r_{11}\gamma_{12}n^2 + m\gamma_{13}r_{11}^C + n\gamma_{14}r_{11}^D}{4r_{11}\beta^2(m^2 + \alpha\beta^2 n^2)} \tag{3.134}$$

$$\lambda_x^{(2)} = \frac{\beta^2}{m^2 + \alpha\beta^2 n^2}\left(\frac{m^4}{64\gamma_{25}} + \frac{n^4}{64}\right) \tag{3.135}$$

$$\lambda_x^{(4)} = -\frac{1}{m^2 + \alpha\beta^2 n^2}\left[\begin{array}{l}\left(\frac{r_{31}^A}{r_{31}}\frac{n^4}{32} + \frac{r_{13}^A}{r_{13}}\frac{m^4}{32\gamma_{25}}\right)\beta^2 \\ + \left(\frac{r_{13}^A}{r_{13}}\frac{m^2}{64n^2\gamma_{25}} + \frac{r_{31}^A}{r_{31}}\frac{n^2}{64m^2}\right)\end{array}\right] \tag{3.136}$$

The coefficients $b_{00}^{(0)}$ and $B_{00}^{(0)}$ need to be calculated, from equation (3.132) the coefficients B_{00}^k and b_{00}^k in equations (3.126) and (3.127) have the relations:

$$b_{00}^k = \alpha\beta^2 B_{00}^k \quad \text{Where k= 0, 2, 4, 6, ..} \tag{3.137}$$

By using equations (3.79) and (3.137) b_{00}^{k} and B_{00}^{k} can be calculated:

$$b_{00}^{(0)} = \frac{\alpha(r_{11}\gamma_{11}m^2 + r_{11}\gamma_{12}n^2 + m\gamma_{13}r_{11}^{C} + n\gamma_{14}r_{11}^{D})}{r_{11}(m^2 + \alpha\beta^2 n^2)} \tag{3.138}$$

$$B_{00}^{(0)} = \frac{r_{11}\gamma_{11}m^2 + r_{11}\gamma_{12}n^2 + m\gamma_{13}r_{11}^{C} + n\gamma_{14}r_{11}^{D}}{r_{11}\beta^2(m^2 + \alpha\beta^2 n^2)} \tag{3.139}$$

Equations (3.133)-(3.139) can be employed to process numerical examination to trace post-buckling equilibrium paths of a graphite-epoxy laminated plate under biaxial compression. It should be shown that equation (3.133) is valid for the post-buckling analysis of laminated structure under uniaxial compressive load by setting α = 0.

The dimensionless load parameter:

$$\lambda_0 = \frac{N_x b}{(E_2 h^3)} \tag{3.140}$$

Where N_x is defined in an equation (3.49).

It can be determined the critical buckling load from equation (3.133) at W_{0m}=0 under uniaxial and biaxial compressive loads, that leads to:

$$\lambda_x = \lambda_x^{(0)} = \lambda_{\mathrm{cr}} \tag{3.141}$$

With equations (3.141) and (3.49), the dimensionless critical buckling loads of structure are:

$$\lambda_{\mathrm{cr}} = \frac{N_{\mathrm{cr}} b}{\left[\pi^2 (D_{11}^{*} D_{22}^{*})^{\frac{1}{2}}\right]} \tag{3.142}$$

The summary of this chapter is divided into two sections, in the first section the basic equations for the static buckling behavior are derived by utilizing (FSDT), then in a second section, these equations are solved by using a two-step perturbation method with the application the boundary conditions, at last, the nonlinear differential equation for the suggested models is obtained. The buckling mode in all cases is taken (m, n) = (1,1).

CHAPTER FOUR

RESULTS AND DISCUSSIONS

CHAPTER FOUR

RESULTS AND DISCUSSION

4.1 INTRODUCTION

In this chapter, the buckling and post-buckling behaviors of graphite/epoxy laminated plates under the uniaxial and biaxial compressive loads are studied. To ensure the accuracy of the current formulation and solution procedure, a validation study will be offered. Thereafter, sundry tabular and graphical data will be showed to study the effects of different parameters on the buckling and post-buckling behaviors of a structure through a comprehensive parametric examination. The simply supported boundary conditions are employed for a laminated composite plate at all edges. Thus, the results are shown under this condition.

4.2 NUMERICAL DATA VERIFICATIONS

As far as it is known that there are no publications about buckling and post-buckling for the graphite/epoxy laminated plates by adopting the two-step perturbation method. Simply supported functionally graded multilayer graphene nano platelet-reinforced polymer composite plate GPLRC under to different loading are taken as an example to validate this study. This section will present the dimensionless critical buckling load with theoretical results of (GPLRC), given by Ref. (Song et al., 2017) [33].

The following geometric parameters of (GPLRC) are:

a= 0.45 m, b= a, h= 0.045 m, V_M= 0.34, E_M= 3.0 GPa, V_{GPL}= 0.186, E_{GPL}= 1.01TPa, $l_{GPL} = 2.5\ \mu m$, $h_{GPL} = 1.5nm$, $w_{GPL} = 1.5\ \mu m$, the weight fraction is 1.0%, epoxy is used to be the matrix material.

As shown in Tables (4-1) and (4-2), good agreements are obtained in these comparisons. According to the comparisons in Tables (4-1) and (4-2), it is clear that the present approach shows an excellent agreement with the previously published study, and this is considered evidence for verifying the accuracy and reliability of the present study.

Table 4-1: Comparison between the results of dimensionless critical buckling load for the GPLRC under uni-axial and equal bi-axial compressive loads and the present study.

Type of loading	α	Dimensionless critical buckling loads (λ_{cr})		
		Reference [33]	Present model	Difference (%)
Uni-axial	**0**	19.465	19.487	0.11%
Bi-axial	**1**	9.690	9.743	0.54%

Table 4-2: Comparison between the results of dimensionless critical buckling load under unequal biaxial loads with different α and the present study.

Type of loading	α	Dimensionless critical buckling loads (λ_{cr})		
		Reference [33]	Present study	Difference (%)
Unequal bi-axial	**-0.4**	32.413	32.138	0.84%
	-0.2	24.310	24.358	0.19%
	0.2	16.379	16.239	0.85%
	0.4	13.965	13.920	0.32%

4.3 NUMERICAL RESULTS FOR STABILITY

4.3.1 INTRODUCTION

In this section, the buckling and post-buckling behavior of the laminated composite plate subjected to different compressive loads are studied. Employing the Two-Step perturbation technique, the equations of motion are solved.

The orthotropic material properties are modeled a graphite/epoxy for the laminated composite plate as follows: E_1= 141Gpa, E_2= 13.1Gpa, G_{12}= 9.31, v_{12}=0.28, G_{13}= G_{23}= G_{12}, which are taken from Ref. (Singha at el., 2001) [49]. Asymmetric cross-ply (0/90/0/90/0/0/90/0/90/0) laminated composite plates are taken with geometric factors are selected as follows: h=0.045m, a= 0.45m, b=a. The number of layers (N) equal to 10, is used in all the numerical calculations.

4.3.2 BUCKLING ANALYSIS

The first stage is to carry out the linear buckling analysis to find critical buckling loads(λ_{cr}). The non-dimensional critical buckling loads of

laminated composite plates are:

$$\lambda_{\mathrm{cr}} = \frac{N_{\mathrm{cr}} b}{\left[\pi^2 (D_{11}^* D_{22}^*)^{\frac{1}{2}}\right]}$$

4.3.3 EFFECT OF VARIOUS MECHANICAL LOADS ON THE CRITICAL BUCKLING LOADS

The critical buckling loads of graphite/epoxy laminated plates under different loadings are exhibited in a Table (4-3). It should be known that $\alpha < 0$, $\alpha = 0$, agree to the plate compressed in the *x*-coordinate, at the plate subjected to uniaxial compressive load in the *x*-coordinate, respectively. Also, $\alpha > 0$ and $\alpha = 1$ mean the plate compressed in the y-direction, and the plate under equal biaxial compression in x and y directions, respectively.

Compared with the uniaxially compressed plate ($\alpha = 0$), the utilization of a bigger compressive load in the x-coordinate can considerably increase the critical buckling loads of the plate. The presence of the larger compressive load in the y-coordinate or equal compressive loads in two directions leads to significantly reduced critical buckling loads.

Table 4-3: Critical buckling loads of laminated composite plates under various compression loads

Mechanical loads	α	Critical buckling loads (λ_{cr})
Equal biaxial	**1**	54.47
Unequal biaxial	**0.5**	72.63
Uniaxial	**0**	108.9
Unequal biaxial	**-0.5**	217.9

4.3.4 EFFECT OF THE RATIO (a/h) ON CRITICAL BUCKLING LOADS UNDER UNIAXIAL And BIAXIAL LOADS

Tables (4-4) and (4-5) show the influence of the length to thickness ratio (a/h) on the dimensionless critical buckling loads in uniaxial and biaxial loading conditions, respectively. Five values of length to thickness ratio are studied (a/h=5, a/h=10, a/h=15, a/h=20, a/h=25).

In both cases of loading, the results explained that the dimensionless critical buckling loads (λ_{cr}) increase with increasing the length to thickness ratio (a/h), and above a/h =15, the change of critical buckling loads is very limited. Also, from the tables (4-4) and (4-5), it is found that the dimensionless critical buckling loads (λ_{cr}) are higher for uniaxial loading.

Table 4-4: Critical buckling loads of laminated composite plates under uniaxial compression loads

α	a/h	Critical buckling loads (λ_{cr})
0	**5**	100.4
	10	108.9
	15	110.7
	20	111.3
	25	111.6

Table 4-5: Critical buckling loads of laminated composite plates under equal biaxial compression loads

α	a/h	Critical buckling loads (λ_{cr})
1	**5**	50.18
	10	54.47
	15	55.34
	20	55.66
	25	55.8

4.4 POST-BUCKLING ANALYSIS

In this section, a post-buckling analysis will be offered for the graphite/epoxy laminated plate. The dimensionless load parameter (λ_0) against the dimensionless maximum deflection W_{0m} results are presented.

Where:

$$\lambda_0 = \frac{N_x b}{(E_2 h^3)}$$

4.4.1 EFFECT OF THE VARIOUS MECHANICAL LOADS ON POST-BUCKLING EQUILIBRIUM PATHS

Figure (4-1) presents the effect of different loadings on the post-buckling behavior of symmetric laminated composite plates. As can be seen, compared with the uniaxially compressed plate (α= 0), the resistance of the structure increases when the use of a compressive force in (α< 0). While the post-buckling resistance reduces of the structure under the equal compressive loads (α= 1) or the large compressive loads in the y-direction (α > 0).

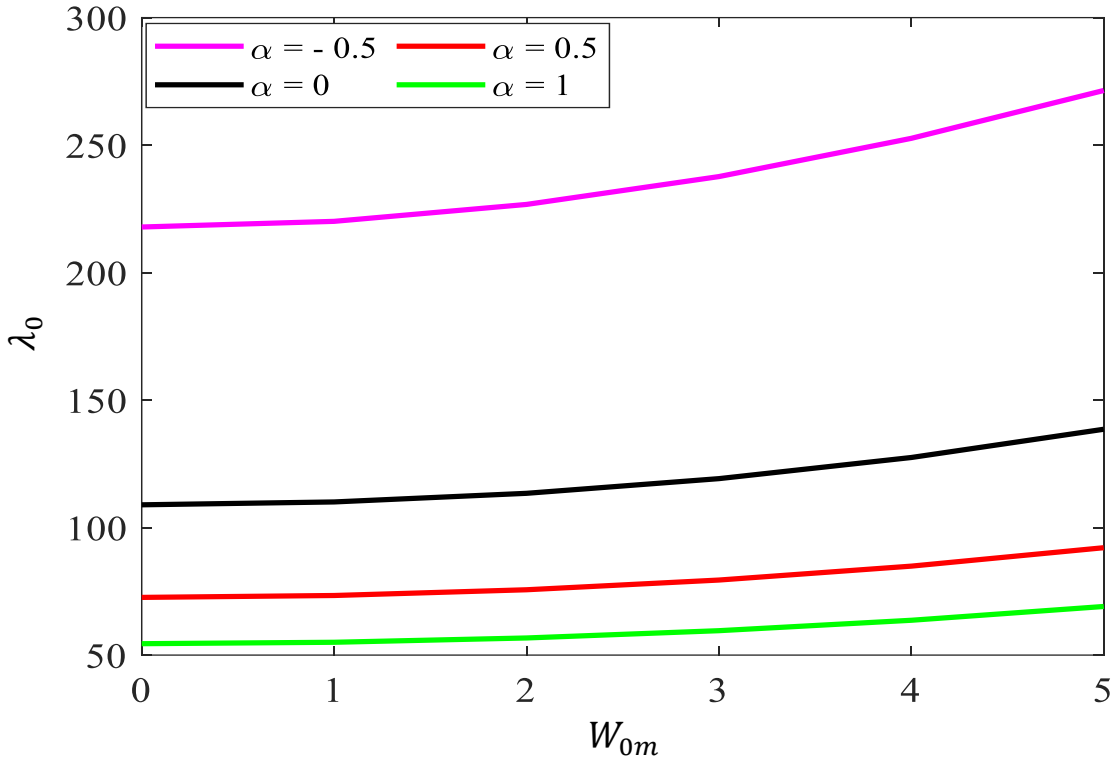

Figure 4-1: Post buckling equilibrium paths of laminated composite plates under biaxial compression loads with different α

4.4.2 EFFECT OF THE RATIO (a/h) ON POST-BUCKLING EQUILIBRIUM PATHS UNDER UNIAXIAL And BIAXIAL LOADS

The effect in uniaxial and biaxial loading conditions, with length to thickness ratio a/h varying from 5 to 25 is investigated and the obtained results are shown in Figures (4-2) and (4-3).

It is found that the resistance of post-buckling is higher for uniaxial loading. For both cases of loading, the resistance of laminated composite plates increases with the ratio a/h increases. Also, it is shown above the ratio a/h equal to15, the variation of post-buckling equilibrium paths loads is very low.

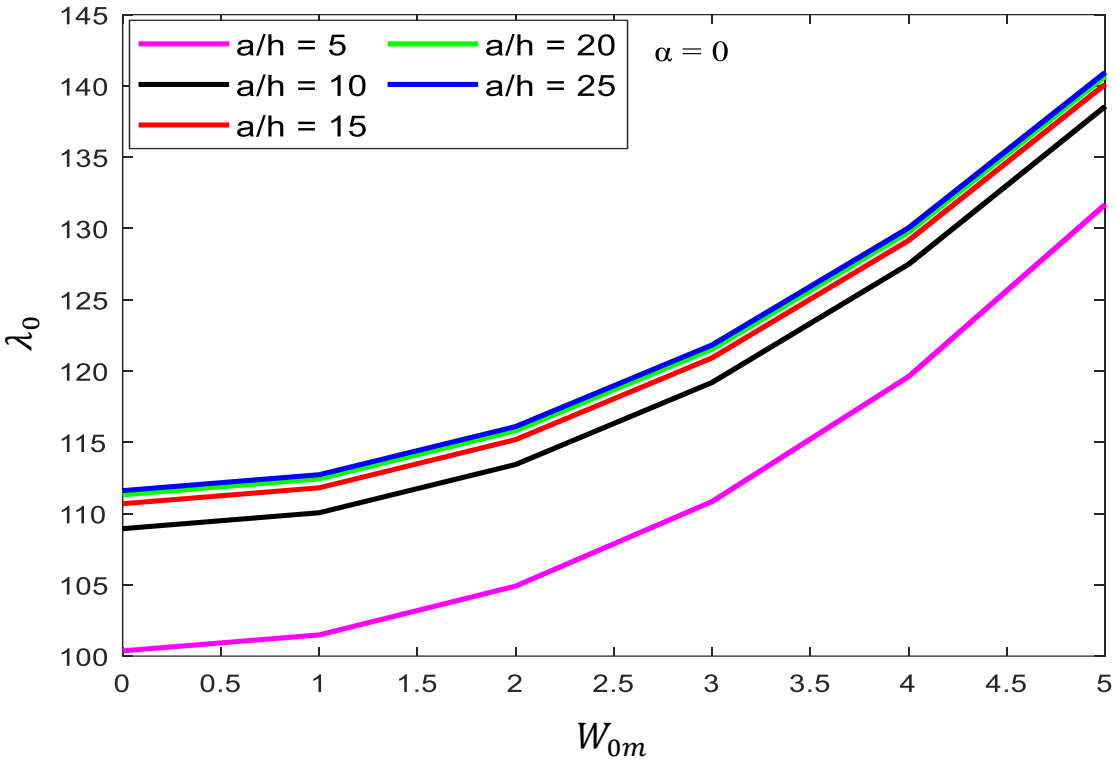

Figure 4-2: Post buckling equilibrium paths of laminated composite plates under uniaxial compression loads

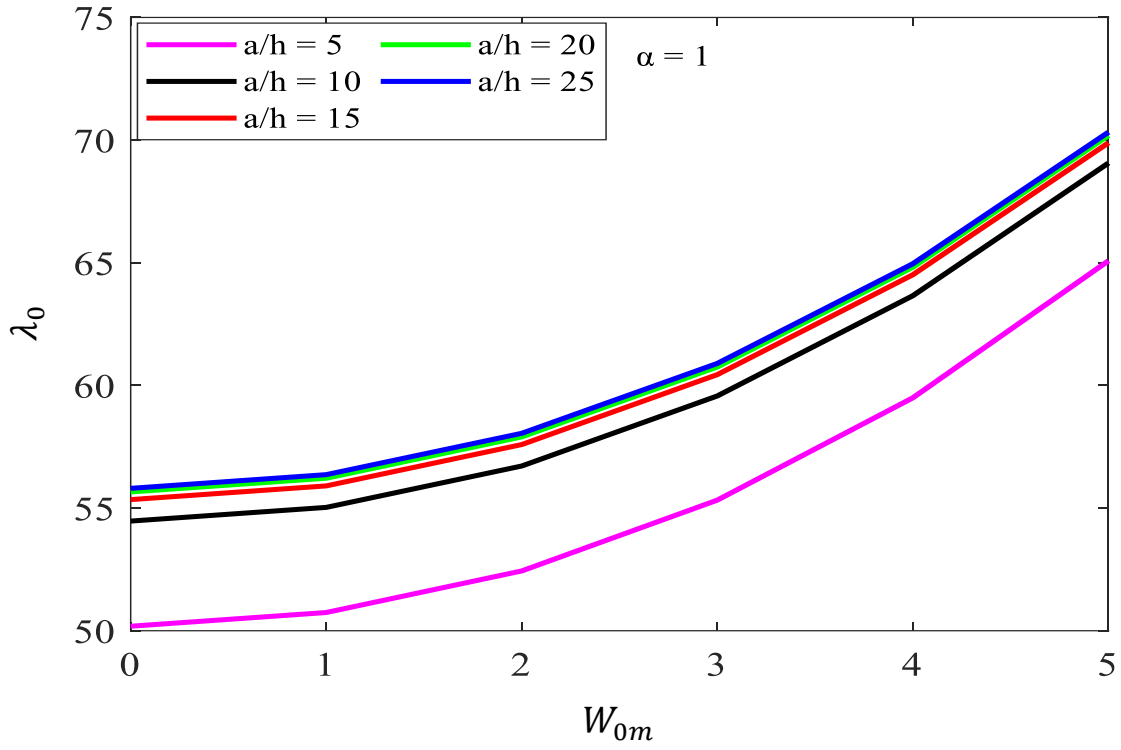

Figure 4-3: Post buckling equilibrium paths of laminated composite plates under biaxial compression loads

CHAPTER FIVE

CONCLUSIONS And RECOMMENDATIONS

And

FUTURE WORK

CHAPTER FIVE
CONCLUSIONS AND RECOMMENDATIONS

5.1 INTRODUCTION

In this research, buckling and post-buckling analyses for symmetric cross-ply laminated composite plates subjected to mechanical loads are obtained based on lamination plate theory (FSDT). In this order, a two-step perturbation technique and simply supported boundary conditions for laminated plates were applied. Effects of various parameters on critical buckling loads and post-buckling equilibrium paths of laminated composite such as different mechanical loads, and length to thicknesses ratio (a/h).

5.2 Conclusions

The key conclusions from the presented results are summarized in the following points:

- ✓ It is found that a two-step perturbation technique is in good agreement with the theoretical analysis results.
- ✓ Compared with the uniaxial compressive load in the x-direction (α= 0), the utilization of unequal biaxial compressive loads in the x-direction (α = -0.5) increases the critical buckling loads and post-buckling resistance of the plate. When the laminated plates are under unequal biaxial compressive load in the y-direction (α = 0.5), or the plate under equal biaxial compression (α= 1) leads to a decrease in the critical buckling loads and post-buckling resistance of the structure.

- ✓ For both uniaxial and biaxial compressive loading cases with the a/h ratio is increased, the dimensionless critical buckling loads and dimensionless load parameter increases. Also, the variation of critical buckling loads and post-buckling equilibrium paths are less above a/h=15.

- ✓ In all cases, it is showed that uniaxial loading has higher critical buckling loads and post-buckling resistance than corresponding equal biaxial loading.

5.3 Recommendations and future work

In this research, the first-order shear deformation theory was utilized to derive the motion equations for laminated composite plates. The research can be widened through the following suggestions:

- ✓ Study the nonlinear stability of the structure by using anti-symmetric-angle ply composite plates.
- ✓ Investigate the stability of the laminated plates under thermal loading.
- ✓ Examine the effect of initial geometric imperfection on the buckling and post-buckling behavior of the structure.
- ✓ Study the effect of number of layers, the orientation of fibers, boundary conditions, on the stability behavior of the laminated composite plates.

REFERENCES

[1] UnuthuReddy, J. N. (2003) Mechanics of laminated composite plates and shells: theory and analysis. CRC press.

[2] Pastuszak, P. D. and Muc, A. (2013) ‘Application of composite materials in modern constructions’, Key Engineering Materials. Trans Tech Publ, pp. 119–129.

[3] Rana, S., Parveen, S. and Fangueiro, R. (2017) ‘13 Advanced Carbon Nanotube Reinforced Multiscale Composites’, in Advanced Composite Materials: Properties and Applications. Sciendo Migration, pp. 545–578.

[4] Ye, J. (2002) Laminated composite plates and shells: 3D modelling. Springer Science & Business Media.

[5] Suliman, B. S. (2018) ‘A hybrid exact strip and finite element method for modelling damage in composite plates’. Cardiff University.

[6] Daniel, I. M., Ishai, O., Daniel, I. M., and Daniel, I. (2006) Engineering mechanics of composite materials. Oxford university press New York.

[7] Moubayed, N., Wahab, A., Bernard, M., El- Khatib, H.,Sayegh, A., Alsaleh, F., and Chehadeh, N. (2014) ‘Static analysis of an orthotropic plate’ Physics Procedia, 55, pp. 367–372.

[8] Turnock, S. R., Keane, A. J., Bressloff, N.W., Nicholls-Lee, R.F., and Boyd, S.W. (2009) ‘Morphing of ‘flying’shapes for autonomous underwater and aerial vehicles’.

[9] Zhang, J., Zhang, W.-H. and Zhu, J.-H. (2011) ‘An extended stress-based method for orientation angle optimization of laminated composite structures’, Acta Mechanica Sinica, 27(6), pp. 977–985.

[10] Yao, S.-S.Jiang, D.,Zhang, Q.Z., and Wang, X.X. (2020) ‘Preparation and Properties of Graphite/Epoxy Resin Conductive Composites’, in IOP Conference Series: Materials Science and Engineering. IOP Publishing, p. 12064

[11] Haugen, M. S. (2012) ‘Non-linear buckling analysis for ultimate limit strength calculations of doubler plate repair on a damaged ship structure’.

[12] Ngamkhanong, C., Wey, C. M. and Kaewunruen, S. (2020) ‘Buckling Analysis of Interspersed Railway Tracks’, Applied Sciences, 10(9), p. 3091.

[13] Vaikunthbhai, K. P. (2014) ‘Free Vibration and Buckling Behaviour of Laminated Composite Panel under Thermal and Mechanical Loading’.

[14] Vrabie, M., Chiriac, R. and Băetu, S. A. (2017) ‘Studies regarding the shear correction factor in the Mindlin plate theory for sandwich plates’, in Advanced Engineering Forum. Trans Tech Publ, pp. 301–308.

[15] Shen, H.-S. (2013) A two-step perturbation method in nonlinear analysis of beams, plates and shells. John Wiley & Sons.

[16] Baba, B. O. and Baltaci, A. (2007) 'Buckling characteristics of symmetrically and antisymmetrically laminated composite plates with central cutout', Applied Composite Materials, 14(4), pp. 265–276.

[17] Kumar, R. A., Jacob, C. V., Lakshminarayana, N., Puneeth, B. M., and Nagabhushana, M. (2009) 'Buckling analysis of woven glass epoxy laminated composite plate', M Tech Thesis NIT Rourkela.

[18] Tu, T. M., Hoa, L. K., Hung, D. X., and Hai, L. T.. (2020) 'Nonlinear buckling and post-buckling analysis of imperfect porous plates under mechanical loads', Journal of Sandwich Structures and Materials, 22(6), pp. 1910–1930.

[19] Hu, H., Badir, A. and Abatan, A. (2003) 'Buckling behavior of a graphite/epoxy composite plate under parabolic variation of axial loads', International journal of mechanical sciences, 45(6–7), pp. 1135–1147.

[20] Wankhade, R. L. and Niyogi, S. B. (2020) 'Buckling analysis of symmetric laminated composite plates for various thickness ratios and modes', Innovative Infrastructure Solutions, 5(3), pp. 1–12.

[21] Fernandes, R. J. and Mirje, K. S. (2018) 'Buckling Analysis of Laminated Composite Plate Using Finite Element Software', International Journal of Civil Engineering Research, 9(1), pp. 11–19.

[22] Kulkarni, K. and Dhurvey, P. (2014) 'Postbuckling analysis of laminated composite plates subjected to in-plane uniaxial load', in

2014 International Conference on Advances in Engineering and Technology Research (ICAETR-2014). IEEE, pp. 1–8.

[23] Sreehari, V. M. and Maiti, D. K. (2015) 'Buckling and post buckling analysis of laminated composite plates in hygrothermal environment using an Inverse Hyperbolic Shear Deformation Theory', Composite Structures, 129, pp. 250–255.

[24] Majeed, W. I. and Tayeh, F. H. (2015) 'Stability and Dynamic Analysis of Laminated Composite Plates', Journal of Engineering, 21(8), pp. 139–159.

[25] Lengvarský, P., Bocko, J. and Hagara, M. (2016) 'The buckling analysis of the composite plates with different orientations of layers', American Journal of Mechanical Engineering, 4(7), pp. 413–417.

[26] Torabizadeh, M. A. (2015) 'Buckling of the composite laminates under mechanical loads with different layups using different plate Advanced Composites Letters, 24(1), p. 096369351502400103.

[27] Osman, M. Y. and Suleiman, O. M. E. (2017) 'Buckling analysis of thin laminated composite plates using finite element method', International Journal of Engineering Research and Advanced Technology (IJERAT), 3(3), pp. 1–18.

[28] Ferreira, A. J. M., Castro, L. M., Roque, C. M. C., Reddy, J. N., and Bertoluzza, S. (2011) 'Buckling analysis of laminated plates by wavelets', Computers and structures, 89(7–8), pp. 626–630.

[29] Shukla, K. K., Nath, Y., Kreuzer, E., and Kumar, K. V. (2005) 'Buckling of laminated composite rectangular plates', Journal of aerospace engineering, 18(4), pp. 215–223.

[30] El Bouhmidi, A. and Rougui, M. (2018) 'Analysis of buckling phenomenon of rectangular laminated plates with a hole under different boundary conditions', in MATEC Web of Conferences. EDP Sciences, p. 2013.

[31] Shadmehri, F., Hoa, S. V and Hojjati, M. (2012) 'Buckling of conical composite shells', Composite Structures, 94(2), pp. 787–792.

[32] DOĞAN, A. (2020) 'Buckling analysis of laminated composite plates under the effect of uniaxial and biaxial loads', Turkish Journal of Engineering, 4(4), pp. 218–225103

[33] Song, M. Yang, J., Kitipornchai, S., and Zhu, W. (2017) 'Buckling and postbuckling of biaxially compressed functionally graded multilayer graphene nanoplatelet-reinforced polymer composite plates', International Journal of Mechanical Sciences, 131, pp. 345–355.

[34] Shen, H.-S. (2009) 'A comparison of buckling and postbuckling behavior of FGM plates with piezoelectric fiber reinforced composite actuators', Composite Structures, 91(3), pp. 375–384.

[35] Shen, H.-S., Xiang, Y., Lin, F., and Hui, D. (2017) 'Buckling and postbuckling of functionally graded graphene-reinforced composite

laminated plates in thermal environments', Composites Part B: Engineering, 119, pp. 67–78.

[36] Li, Z.-M., Liu, T. and Yang, D.-Q. (2018) 'Postbuckling behavior of shear deformable anisotropic laminated cylindrical shell under combined external pressure and axial compression', Composite Structures, 198, pp. 84–108.

[37] Shen, H.-S. and Xiang, Y. (2018) 'Postbuckling behavior of functionally graded graphene-reinforced composite laminated cylindrical shells under axial compression in thermal environments', Computer Methods in Applied Mechanics and Engineering, 330, pp. 64–82

[38] Fan, Y. and Wang, H. (2016) 'Thermal postbuckling and vibration of postbuckled matrix cracked hybrid laminated plates containing carbon nanotube reinforced composite layers on elastic foundation', Composite Structures, 157, pp. 386–397.

[39] Shen, H.-S. and Li, Q. S. (2004) 'Postbuckling of shear deformable laminated plates resting on a tensionless elastic foundation subjected to mechanical or thermal loading', International Journal of Solids and Structures, 41(16–17), pp. 4769–4785.

[40] Shen, H.-S. and Xiang, Y. (2019) 'Thermal buckling and postbuckling behavior of FG-GRC laminated cylindrical shells with temperature-dependent material properties', Meccanica, 54(1), pp. 283–297.

[41] Bhaskar, D. P. and Thakur, A. G. (2019) ‘FE modeling for geometrically nonlinear analysis of laminated plates using a new plate theory’, Advances in aircraft and spacecraft science, 6(5), pp. 409–426.

[42] Li, D. and Kim, I. Y. (2020) ‘Modified element stacking method for multi-material topology optimization with anisotropic materials’, Structural and Multidisciplinary Optimization, 61(2), pp. 525–541.

[43] Alieldin, S. S., Alshorbagy, A. E. and Shaat, M. (2011) ‘A first-order shear deformation finite element model for elastostatic analysis of laminated composite plates and the equivalent functionally graded plates’, Ain Shams Engineering Journal, 2(1), pp. 53–62.

[44] Ovesy, H. R. and Kharazi, M. (2011) ‘Stability analysis of composite plates with through-the-width delamination’, Journal of engineering mechanics, 137(2), pp. 87–100.

[45] Roylance, D. (2000) ‘Laminated composite plates’, Massachusetts Institute of Technology Cambridge.

[46] Namdar, Ö. and Darendeliler, H. (2017) ‘Buckling, postbuckling and progressive failure analyses of composite laminated plates under compressive loading’, Composites Part B: Engineering, 120, pp. 143–151.

[47] Domfang, M. C. (2013) ‘Analysis of Laminated Anisotropic Plates and Shells Via a Modified Complementary Energy Principle

Approach'. Via a Modified Complementary Energy Principle Approach," 2013.

[48] Javaheri, R. and Eslami, M. R. (2002) 'Thermal buckling of functionally graded plates based on higher order theory', Journal of thermal stresses, 25(7), pp. 603–625.

[49] Singha, M. K., Ramachandra, L. S. and Bandyopadhyay, J. N. (2001) 'Thermal postbuckling analysis of laminated composite plates', Composite Structures, 54(4), pp. 453–458.

APPENDICES

Appendix A

The differential operators in Equations (3.54)-(3.57) as the following:

$$L_{01} = \gamma_{11}\frac{\partial^2}{\partial x^2} + \gamma_{12}\frac{\partial^2}{\partial y^2}$$

$$L_{02} = \gamma_{13}\frac{\partial}{\partial x}$$

$$L_{03} = \gamma_{14}\frac{\partial}{\partial y}$$

$$L_{04} = \gamma_{15}\frac{\partial}{\partial x}$$

$$L_{05} = \frac{\partial^2}{\partial x^2} + \gamma_{16}\frac{\partial^2}{\partial y^2} + \gamma_{17}$$

$$L_{06} = \gamma_{18}\frac{\partial^2}{\partial x\,\partial y}$$

$$L_{07} = \gamma_{19}\frac{\partial}{\partial y}$$

$$L_{08} = \gamma_{20}\frac{\partial^2}{\partial x\,\partial y}$$

$$L_{09} = \gamma_{21}\frac{\partial^2}{\partial x^2} + \gamma_{22}\frac{\partial^2}{\partial y^2} + \gamma_{23}$$

$$L_{10} = \frac{\partial^4}{\partial x^4} + \gamma_{24}\frac{\partial^4}{\partial x^2\,\partial y^2} + \gamma_{25}\frac{\partial^4}{\partial y^4}$$

In which:

$$[\gamma_{11}, \gamma_{12}] = \frac{k_S a^2 [A_{55}, \beta^2 A_{44}]}{(\pi^2 D_{11}^*)}$$

$$\gamma_{13} = \frac{k_S A_{55} a^2}{(\pi^2 D_{11}^*)}$$

$$\gamma_{14} = \frac{k_S \beta A_{44} a^2}{(\pi^2 D_{11}^*)}$$

$$\gamma_{15} = -\frac{k_S A_{55} a^2}{(\pi^2 D_{11}^*)}$$

$$[\gamma_{16}, \gamma_{17}] = \frac{[\pi^2 \beta^2 D_{66}^*, -k_S A_{55} a^2]}{(\pi^2 D_{11}^*)}$$

$$\gamma_{18} = \frac{\beta (D_{12}^* + D_{66}^*)}{D_{11}^*}$$

$$\gamma_{19} = -\frac{k_S \beta a^2 A_{44}}{(\pi^2 D_{11}^*)}$$

$$\gamma_{20} = \frac{\beta (D_{12}^* + D_{66}^*)}{D_{11}^*}$$

$$[\gamma_{21}, \gamma_{22}, \gamma_{23}] = [\pi^2 D_{66}^*, \pi^2 \beta^2 D_{22}^*, -k_S A_{44} a^2] / \pi^2 D_{11}^*$$

$$[\gamma_{24}, \gamma_{25}] = \frac{\beta^2 [2A_{12}^* + A_{66}, \beta^2 A_{11}^*]}{A_{22}^*}$$

APPENDIX B

Excepting $b_{00}^{(k)}$ and $b_{00}^{(k)}$, the Coefficients are offered in equations (3.114)-(3.121) as following:

$$r_{11}^{C} = (m\gamma_{15})(m^2\gamma_{21} + n^2\gamma_{22} - \gamma_{23}) - (mn\gamma_{18})(n\gamma_{19})$$

$$r_{11}^{D} = (m^2 + n^2\gamma_{16} - \gamma_{32})(n\gamma_{19}) - (m\gamma_{15})(mn\gamma_{20})$$

$$r_{11} = (m^2 + n^2\gamma_{16} - \gamma_{17})\,(m^2\gamma_{21} + n^2\gamma_{22} - \gamma_{23}) -(\,mn\gamma_{18})\,(\,mn\gamma_{20})$$

$$r_{13}^{A} = \frac{\beta^4 m^4}{16\gamma_{25}}\,[(m^2 + 9\gamma_{16}n^2 - \gamma_{17})(m^2 + 9\gamma_{22}n^2 - \gamma_{23}) - (3mn\gamma_{18})(3mn\gamma_{20})]$$

$$r_{13}^{C} = \frac{\beta^4 m^4}{16\gamma_{214}}\,[(m\gamma_{15})(\gamma_{21}m^2 + 9\gamma_{22}n^2 - \gamma_{23}) - (3n\gamma_{19})(3mn\gamma_{18})]$$

$$r_{13}^{D} = \frac{\beta^4 m^4}{16\gamma_{25}}[\,(3n\gamma_{19})(\,m^2 + 9\gamma_{16}n^2{-}\gamma_{17}) - (m\gamma_{15})(\,3mn\gamma_{20})]$$

$$r_{13} = [(m^2\gamma_{11} + 9n^2\gamma_{12} - m^2\beta^2 B_{00}^{(0)} - 9n^2\beta^2 b_{00}^{(0)})[\,(m^2 + 9\gamma_{16}n^2{-}\gamma_{17})(\gamma_{21}m^2 + 9\gamma_{22}n^2 - \gamma_{23}) -\ (\,3mn\gamma_{18})(3mn\gamma_{20})]] +$$

$$[(m\gamma_{13})\,[(m\gamma_{15})(\gamma_{21}m^2 + 9\gamma_{22}n^2 -\ \gamma_{23}) - (\,3mn\gamma_{18})(3n\gamma_{19})]]$$

$$+[(\,3n\gamma_{14})[(\,3n\gamma_{19})(\,m^2 + 9\gamma_{16}n^2 -\ \ \gamma_{17}) -(3mn\gamma_{20})(\,m\gamma_{15})]]$$

$$r_{31}^{A} = \frac{\beta^4 n^4}{16}[(9m^2{+}\gamma_{16}n^2 - \gamma_{17})(9\gamma_{21}m^2 + \gamma_{22}n^2 - \gamma_{23}) - (3mn\gamma_{18})(3mn\gamma_{20})]$$

$$r_{31}^{C} = \frac{\beta^4 n^4}{16}\,[(3m\gamma_{15})(9\gamma_{21}m^2 + \gamma_{22}n^2 - \gamma_{23}){-}(3mn\gamma_{14})(n\gamma_{19})]$$

$$r_{31}^{D} = \frac{\beta^4 n^4}{16}\ [(n\gamma_{19})(9m^2+\gamma_{16}n^2 - \gamma_{17}) - (3m\gamma_{15})(3mn\gamma_{20})]$$

$$r_{31} = \Big[9m^2\gamma_{11} + n^2\gamma_{12} - 9m^2\beta^2 B_{00}^{(0)} - n^2\beta^2 b_{00}^{(0)}[(9m^2+\gamma_{16}n^2 - \gamma_{17})(9\gamma_{21}m^2 + \gamma_{22}n^2 - \gamma_{23}) - (3mn\gamma_{18})(3mn\gamma_{20})]\Big] + \Big[3m\gamma_{13}[(3m\gamma_{15})(9\gamma_{21}m^2 + \gamma_{22}n^2 - \gamma_{23}) - (3mn\gamma_{18})(n\gamma_{19})]\Big] + [n\gamma_{14}[(n\gamma_{19})(9m^2+\gamma_{16}n^2 - \gamma_{17}) - (3m\gamma_{15})(-3mn\gamma_{20})]]$$

الخلاصة

في البحث الحالي تم فحص الاستقرار الساكن غير الخطي للصفائح الطبقيه المتعامدة تحليليا والتي تتعرض لاحمال ضغط احادية المحور وثنائيه المحور.

تم استخدام الصفائح الرقائقية المركبة المصنوعة من الالياف المقواة احادية الاتجاه (الكرافيت) ومادة (الايبوكسي) التي تستخدم في الهياكل الهندسية المتقدمة.

استنادا الى نظريه تشوه القص من الدرجه الاولى (FSDT) مع الاخذ بنظر الاعتبار الصيغ غير الخطيه من نوع (Von Karman) وبأستخدام مبدأ (Minimum total potential energy) تم الحصـــول على معادلات التوازن والاســـتقرار والتوافق للالواح الطبقيه. بعد ذلك من خلال عرض (Two Step Perturbation Technique) تم حل المعادلات.

تم عرض النتائج على شكل مخططات تعرض التباين في معاملات حمل الانبعاج غير البعدية مع اقصى انحراف بلا ابعاد تم مقارنة نتائج الدراسة الحالية بنتائج الدراسات السابقة والتي قدمت توافقا جيدا مع النتائج الحالية.

اضافة الى ذلك تم دراسة تاثير العديد من المعاملات مثل الاحمال ثنائية المحور المختلفة، ونسبة الطول الى السمك على احمال الانبعاج الحرجة ومسارات التوازن بعد الانبعاج للصفائح الطبقية بدقة.

من النتائج ، كان الحد الأقصـى لأحمال الأنبعاج الحرجة ٢١٧,٩ و ١١١,٦ تحت أحمال ضـغط ثنائية المحور غير متســاوية ، وتحت الحمل أحادي المحور عند (الطول/الســمك) = ٢٥، على التوالي. كذلك اقصـى مقاومة مابعد الأنبعاج كانت عند نفس الحالات التي يكون فيها اقصـى حمل أنبعاج.

وزارة التعليم العالي والبحث العلمي

جامعة الانبار

كلية الهندسة

تحليل الأنبعاج ومابعد الأنبعاج لصفيحة مركبة تحت الأحمال الأنضغاطية

رسالة مقدمة

الى كلية الهندسة /جامعة الأنبار

وهي جزء من متطلبات نيل شهادة ماجستير علوم

في

الهندسة الميكانيكية

من قبل

سها هاشم محمد الدوسري

(بكالوريوس علوم في الهندسة الميكانيكية ٢٠٠٧)

بأشراف

أ.م.د حمد محمد حسن

ربيع الأول ١٤٤٣

تشرين الأول ٢٠٢١